Journal of Marine Systems 252 (2025) 104146

Contents lists available at ScienceDirect

Journal of Marine Systems

journal homepage: www.elsevier.com/locate/jmarsys

Shoreline displacement assessment on the Pacific Coast of Colombia using numerical simulations, remote sensing and machine learning in a data-limited environment

Andrés M. Enríquez-Hidalgo [a,*], Andrés Vargas-Luna [b,e], Marc Mestres [c,d], Jorge Escobar-Vargas [b,e], Manuel Espino Infantes [c,d], Andrés Torres [b,e,f]

[a] Faculty of Civil Engineering, Universidad Santo Tómas, Bogotá D.C., Colombia
[b] Civil Engineering Department, Engineering School, Pontificia Universidad Javeriana, Colombia
[c] Laboratori d'Enginyeria Marítima, Universitat Politècnica de Catalunya (LIM/UPC) – Barcelona Tech, Spain
[d] Centro Internacional de Investigación de los Recursos Costeros (CIIRC), Barcelona, Spain
[e] Ciencia e ingeniería del agua y el ambiente Research Group, Pontificia Universidad Javeriana, Colombia
[f] Instituto Javeriano del Agua, Pontificia Universidad Javeriana, Carrera 7ª No. 40-62, Bogotá, Colombia

ARTICLE INFO

Keywords:
Hydrodynamic numerical modeling
SWAN
Shoreline displacement
Remote sensing
Coastsat
Machine learning
Random forest
Tropical Pacific Coast

ABSTRACT

Understanding Shoreline Displacement (SLD) in data- limited coastal regions, is critical for risk-informed management. We evaluate an integrated workflow that couples wave-hydrodynamic modeling, tide-corrected CoastSat satellite shorelines, and machine learning (ML) to characterize SLD drivers in Tumaco Bay on Colombia's southern pacific coast. Using data from 2017 to 2018, various structured meshes and advection schemes are tested. A 100 m mesh with a cyclic advection scheme best reproduced mesotidal dynamics when forced with TPXO8 tidal model for boundary conditions and wind data provided by a meteorological station. Model performance evaluated against Waverys reanalysis and available observations showed good skill, supporting application where in situ data are sparse. Multidecadal (1993–2024) CoastSat shoreline positions for El Morro and El Bajito beaches indicate an overall accretional tendency but found erosion hotspots affecting densely settled and touristic sectors. Regional wave conditions feature significant wave height (H_s) of 0.3–1.1 m, peak wave period (T_p) of 4–18 s, and predominantly westward wave approach, Random Forest (RF) results identify sea level (SL) and mean wave propagation direction (Θm) as the leading contributors to observed SLD variability, whereas H_s and T_p are secondary under the area's moderate wave energy. The study demonstrates the need to monitor localized erosion despite net accretion and demonstrate that combining physics-based modeling, open satellite archives, and data-driven methods can yield policy-relevant coastal insights in data-scarce tropical estuarine environments.

1. Introduction

Coastal zones, housing approximately 23 % of the global population (Choo et al., 2021; Davenport, 2021), stand as pivotal regions with profound societal and ecological significance. These areas, however, face inherent vulnerability to various natural hazards, leading to potential adverse consequences on social, economic, and environmental fronts (Chowdhury et al., 2017; Marsooli et al., 2017). Serving as an interface between the ocean and land, coastal environments are influenced significantly by the forces of waves, tides, and wind energy exposure (Morris et al., 2020; Davenport, 2021; Houghton et al., 2025) causing erosion that leads to the migration of coastlines towards inland areas (Wen et al., 2019). Notably, more than 70 % of coastal areas worldwide are currently dealing with erosion processes (de Andrade et al., 2019). The escalating dynamics of this process observed in various countries have emerged as a major concern, particularly in nations with limited resources (Gomez et al., 2020). This emphasizes the urgent need for effective strategies and tools to comprehensively understand and mitigate the impacts of coastal erosion on vulnerable coastal communities and ecosystems (Enríquez-Hidalgo et al., 2025).

* Corresponding author at: Faculty of Civil Engineering, Universidad Santo Tómas, Bogotá D.C, Colombia.
E-mail addresses: andresenriquez@usta.edu.co (A.M. Enríquez-Hidalgo), avargasl@javeriana.edu.co (A. Vargas-Luna), marc.mestres@upc.edu (M. Mestres), jorge-escobar@javeriana.edu.co (J. Escobar-Vargas), manuel.espino@upc.edu (M.E. Infantes), andres.torres@javeriana.edu.co (A. Torres).

https://doi.org/10.1016/j.jmarsys.2025.104146
Received 17 December 2024; Received in revised form 22 July 2025; Accepted 15 October 2025
Available online 16 October 2025
0924-7963/© 2025 Elsevier B.V. All rights are reserved, including those for text and data mining, AI training, and similar technologies.

SLD, influenced by tidal and wave dynamics, is an aspect of the complex interactions within coastal regions that requires continuous monitoring of changing coastline position (Idier et al., 2019; Son et al., 2020). Understanding wave characteristics is essential for evaluating erosion and accretion, which inform shoreline configurations and changes (Bryant et al., 2022; Viñes et al., 2025). The application of numerical models is therefore imperative, as Martins et al. (2017) highlight, to enhance the precision in assessing coastal risk variables. Such tools contribute significantly to the accuracy and reliability of coastal models, offering a robust basis for the evaluation and management of coastal hazards (Deltares, 2022a, 2022b).

Given the important role that coastal areas play in socio-economic development, particularly in developing regions, where marine instrumentation is scarce and available wave records, if any, are typically limited to very short time periods insufficient for long-term assessment, and recognizing that human activities in these natural environments contribute to accelerated flooding and erosion rates (Niño and Oviedo, 2018; Mury et al., 2020), the creation of artificial wave records is an excellent resource to meet this need. These records should be generated using numerical wave propagation models and analysis of local wind databases. Subsequently, they must be calibrated using any existing instrumentation, and finally processed to asses hazard (Ortega et al., 2013; Rivas et al., 2019; Cano, 2020).

The complexity of coastal erosion processes and the scarcity of localized data in many developing regions, advanced tools like ML are becoming increasingly important. ML, specifically the RF model, allows for the analysis of large datasets by identifying complex patterns in environmental variables, such as wave height, tidal forces, and wind energy, that influence SLD. This technique enhances traditional numerical models by providing predictive insights into erosion rates and coastal variability, even when observational data are sparse or inconsistent (Add relevant references here). The integration of numerical simulations and ML offers a comprehensive approach to mitigating the uncertainties that typically arise in data-limited settings.

The establishment of preventive and mitigative mechanisms in areas prone to coastal hazards can result in significant socio-economic savings as opposed to the costs and complexities involved of relocating vulnerable populations (Romero-Martín et al., 2025; van Dongeren et al., 2018). However, these strategies often lack a comprehensive wave and hydrodynamic analysis, which is a critical component for SLD accurate hazard assessments (Niño and Oviedo, 2018; Bonaldo et al., 2019). The success of these strategies relies on being aligned with the capabilities and needs of the local population during their development (Djouder and Boutiba, 2017; Cano Calvo, 2021; Schipper et al., 2022). This key task requires an approach that includes the results of hydrodynamic and wave simulations and their relationship with the SLD (Lin and Pussella, 2017).

RF model, is becoming an increasingly valuable tool in coastal studies for identifying patterns and causal relationships, providing a deeper understanding of vulnerabilities and threats in coastal zones. Recent efforts have focused on developing advanced image-processing algorithms and automated procedures to increase the precision of shoreline detection and coastal erosion estimation from satellite image analysis (Fogarin et al., 2023). In this context, ML approaches are gaining prominence, not only for their ability to classify land and sea from Earth Observation data but also for distinguishing between surface typologies, such as agriculture, wetlands, and artificial surfaces. Studies using ML for coastal mapping have shown promising results, with models like RF, logistic regression, and neural networks achieving over 99.7 % accuracy in shoreline classification tasks(Arjasakusuma et al., 2021). Furthermore, RF models provide robust analysis by identifying important decision nodes across numerous decision trees, offering insights into variables that influence coastal dynamics, such as risk exposure, socioeconomic factors, and land use (Siders and Keenan, 2020).

Tumaco bay, situated on the Colombian Pacific Coast, and encompassing Tumaco and El Morro Islands, is a region affected by coastal erosion. This erosion leads to the gradual loss of sand barrier islands, compounded by the force of waves and the mesotidal environment (Otero et al., 2014). Moreover, this area is subject to the meteorological influences of the Intertropical Convergence Zone (ITCZ), which, in the early part of the year, facilitates the passage of the Panama jet stream, carrying easterly winds from the Caribbean. In contrast, the latter half of the year sees the absence of this convergence zone, giving way to the Choco jet stream, bringing winds from the southeast that contribute to the area's atmospheric instability (Niño and Oviedo, 2018).

The convergence of environmental challenges, socio-economic issues and cultural aspects in this area presents a particular case study for assessing wave and tidal effects on SLD management in developing and vulnerable communities worldwide. The paucity of data for in-depth analysis, exacerbated by limited governmental support, consistently introduces uncertainty into studies of coastal dynamics (Tejada, 2003; Stronkhorst et al., 2018a). In the Colombian Pacific Basin (CPB), particularly around of Tumaco and El Morro islands, efforts to gauge erosion and accretion processes have relied on remote sensing methods (Niño and Oviedo, 2018) and global open-access data to compensate for the local data shortfall (Stronkhorst et al., 2018b). This lake of data is a widespread issue in many developing countries, where the utility of numerical modeling for estimating wave and tidal processes in hazard management remains underutilized.

This study explores the application of the Simulating Waves Nearshore (SWAN) and FLOW modules in Delft-3D, to obtain 2D data on the mesotidal environment, H_s, T_p, and Θm around Morro and Tumaco islands, and their relationship with the SLD. The aim is to illustrate the use of these numerical and remote sensing tools to measure the influence of coastal forcing on the shoreline of Bajito and Morro beaches. This research employs a ML based on RF to assess the importance of hydrodynamics and wave forcing on SLD and to predict its variability based on these variables.

2. Materials and methods

2.1. Study area

This work was carried out around the coast of Tumaco Bay, located in Nariño-Colombia. The urban area of Tumaco is divided into three zones: Morro Island, Tumaco Island, and the city of San Andres de Tumaco, connected by the Pindo Bridge and the Morro Bridge. A significant number of rivers drain the territory, and there are two major basins influencing the study area: to the north, the basin of the south branch of the Patía river, and to the south, the mouth of the Mira river; in the mid zone, there are several tributaries of micro basins including Tablones, Rosario, Caunapí, Mejicano, Chagüi, Colorado and Curay. San Andres de Tumaco is the main town, the largest of the 64 municipalities in Nariño, and the second most important port on the Colombian Pacific coast. Its population is mainly composed of Afro-Colombian communities and to a lesser extent of indigenous groups (Alcaldía Municipal de Tumaco, 2008).

The characteristics of the area have fostered the development of critical formations such as beaches, banks, bars, high salinity marshes, and soils derived from organic deposits featuring mangrove, guandal, and riparian vegetation. These formations are exposed to average wave heights between 0.5 m and 1.5 m, with periods ranging between 8 s and 10 s, originating from the northwest of the Pacific Ocean, particularly during the Boreal winter months. Observational records and existent studies have indicated significant morphodynamic changes in the low tide zone of Tumaco Bay, including erosion and accretion processes in the El Pindo sector between 1921 and 1948; the erosion of the southern side of the island in 1969; the erosive processes caused by the 1979 tsunami and the storm surge of 1982 and 1983. The impact of these last natural events on the Tumaco island has been greatly diminished by the presence of the El Guano and La Viciosa islands, which have acted as 'protective barriers'. However, the presence of these islands does not provide security for the settlement of houses in this low-tide area, especially if one takes into account that the island of El Guano disappeared during the 1979 tsunami and although it is in the process of formation, once again, has not yet emerged and therefore cannot fulfill its role as a protective element (C. Tejada et al., 2003).

Fig. 1 situates the study area at nested spatial scales and identifies the measurement assets and proxy wave data sources used in this work. Panel (a) shows the Nariño Department in southwest Colombia; the frame outlines the extent of panel (b). Panel (b) zooms to the Tumaco coastal region and marks the Waverys reanalysis extraction point (white circle), used as an alternative wave dataset when local buoy records were incomplete or flagged low-confidence. Panel (c) focuses on Tumaco Bay, indicating the hydrometeorological station that provided sea-level, wind-direction, and wind-speed observations (yellow star), the tide gauge (green polygon), and the RedMPOMM–DIMAR wave buoys (white circles) referenced in this study.

2.2. Collected data

The data collection of coastal bathymetries of Tumaco bay was carried out by the National Hydrographic Service of the General Maritime Directorate, a part of the Defense Ministry of Colombia. The bathymetric survey information is referred to as the Mean Low Water Sprint (MLWS) and is presented in the EPSG:32617 – WGS 84 / UTM zone 17 N projection. The information used is composed of two bathymetry surveys carried out in different years: the 2019 survey covering 18,830 measured points covering 33,232 ha, and the 2020 survey including 2799 measured points covering 5715 ha. These measurements do not cover the surroundings of Tumaco Island and the Tumaco city extension. Therefore, it was necessary to combine these observations with a satellite mapping using reflectance data given by SENTINEL II using Google Earth Engine generating a depth calculation code in shallow water <15 m (Digital Elevation Model) developed in Javascript (Li et al., 2021) the result is showed in Fig. 2.

The raw data collection of marine meteorology parameters was carried out by the Oceanographic and Marine Meteorology Parameter Measurement Network (Mpomm Network-DIMAR), highlighting that the provided data is pre-filtered by the DIMAR personnel to meet their quality standards. The recollected information consists of 31,301 observations of the SL, measured every hour from January 1st, 2011, to December 31st, 2021, 12833 observations of the wind speed and wind direction, measured every six (6) hours from March 18th, 2011, to July 31st, 2020; 311,195 observations of the max wave height, mean wave height, max wave period, mean wave period and Θm, measured hourly from January 1st of 2011 to July 31st of 2020.

Additionally, global data on H_s, T_p, and Θm were downloaded from Copernicus Marine Service using the WAVERYS product. This product is based on the third-generation wave model MFWAM, operating on an irregular grid of 1/5° with a 3-h time step (https://data.marine.copernicus.eu/product/GLOBAL_MULTIYEAR_WAV_001_032/description). It takes into account ocean currents from the GLORYS12 physical ocean reanalysis and assimilates H_s observations from historical altimetry

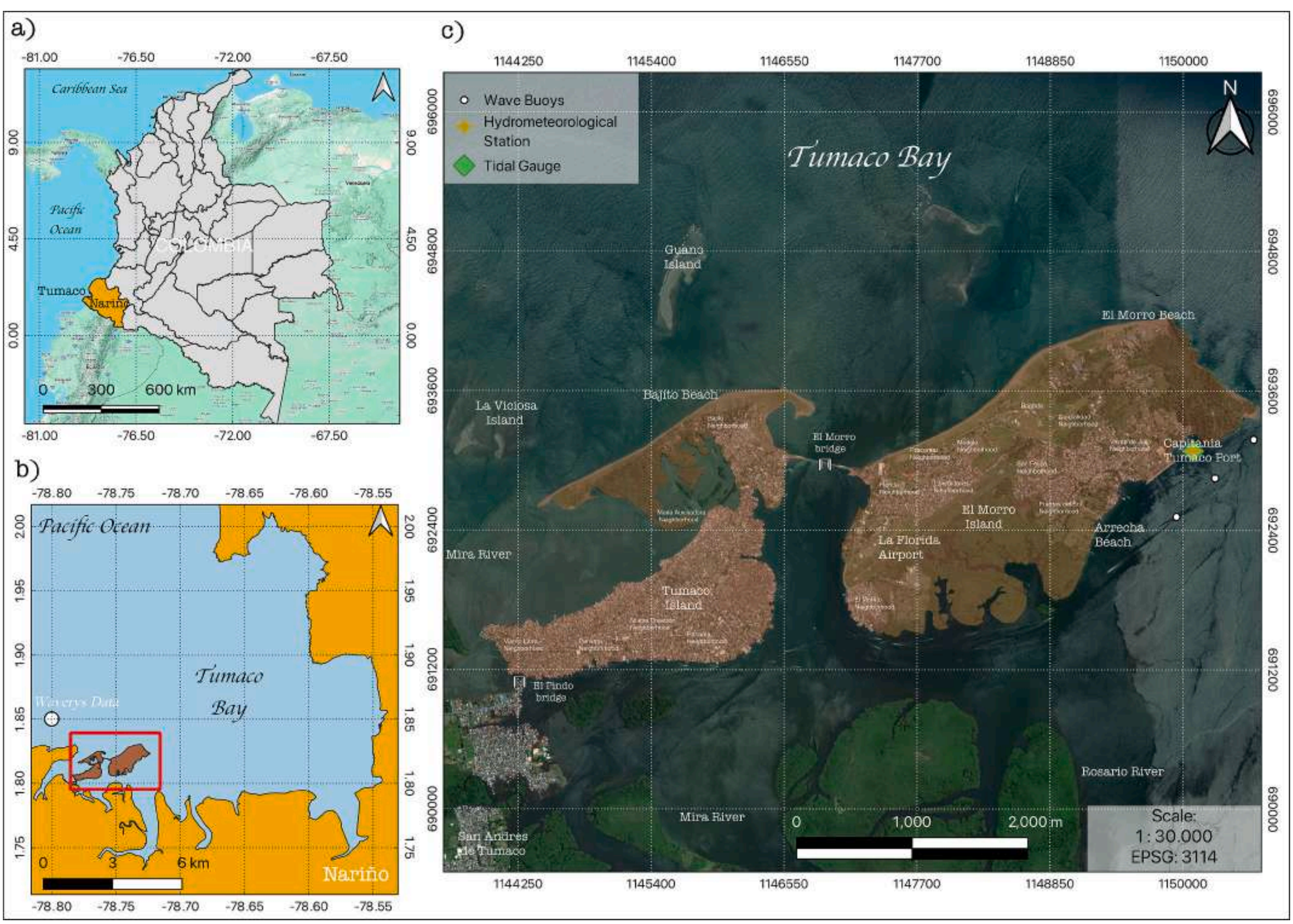

Fig. 1. Location of study area and data sources: a) Nariño Department, southwest Colombia (frame shows extend of panel b; b) Tumaco coastal region with Waverys extraction point; c) Tumaco Bay showing Tumaco and El Morro Islands, hydrometeorological station, tide gauge and wave bouys.

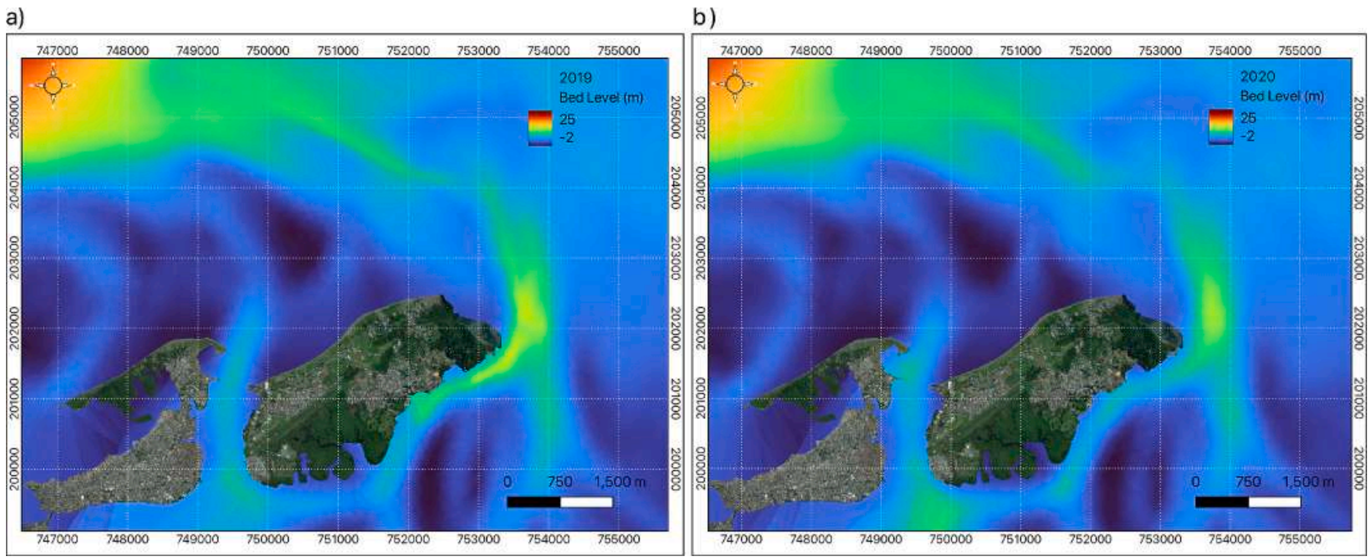

Fig. 2. Bottom topography information of Tumaco bay, for a) 2019, b) 2020.

missions and directional wave spectra from Sentinel-1 SAR since 2017 onwards. The mean sea level (MSL) was obtained from the forecast report of high and low tides on the Colombian Pacific coast through the tide station located in the Fishing Port of Tumaco, department of Nariño, which is made up of a sensor type radar and a transmission system, with a record since 1952 published in IDEAM (2020).

2.3. Numerical modeling

The modeling of coastal areas involves multi-dimensional hydrodynamic and wave simulations, employing non-steady flow and transport formulations based on meteorological and tidal data (Marsooli et al., 2017). These approaches are applicable in multi-disciplinary contexts, utilizing the solution of depth-averaged unsteady shallow water equations. To accurately represent the interactions between waves and currents in coastal regions, it is essential to integrate both hydrodynamic and wave models. This integration allows for a more comprehensive understanding of coastal dynamics by capturing the bidirectional influences between wave and current processes (Martos and Isabel, 2022). In this regard, coupling with the third-generation spectral wave model SWAN has proven to be instrumental when taken into account the effect of flow on the waves (via set-up, current refraction, and enhanced bottom friction) and the effect of waves on current (via forcing, enhanced turbulence, and enhanced bed shear stress) (Paulus et al., 2013). It is recommended to use an online coupling of Delft3D-WAVE with Delft3D-FLOW to consider the two way wave-current interaction process (Deltares, 2022b; Kadigi et al., 2022; Sun et al., 2022). SWAN explicitly represents physics through state-of-the-art formulations, possesses full spectral capability across all frequencies and directions, and maintains unconditional stability due to the implementation of fully explicit schemes (Sun et al., 2022).

SWAN coupled with FLOW was applied in the Delft3D software developed by Deltares in the Netherlands. Delft3D is Open-Source Software that provides the development of the hydrodynamic (Delft3D-FLOW module) and waves (Delft3D-WAVE module) processes in coastal, riverine, estuarine, or lake environments. SWAN model is based on the discrete spectral action balance equation and is fully spectral (in all directions and frequencies). The latter implies that short-crested random wave fields propagating simultaneously from widely different directions can be accommodated (e.g. a wind sea with superimposed swell). SWAN computes the evolution of random, short-crested waves in coastal regions with deep, intermediate, and shallow water and ambient currents. Delft3D-FLOW solves depth-averaged shallow water equations, which consist of the continuity equation, and two horizontal momentum equations (see Eqs. (1) to (3)) (Deltares, 2022a).

$$\frac{\partial\zeta}{\partial t}+\frac{1}{\sqrt{G_{\xi\xi}}\sqrt{G_{\eta\eta}}}\frac{\partial\left((d+\zeta)U\sqrt{G_{\eta\eta}}\right)}{\partial\xi}+\frac{1}{\sqrt{G_{\xi\xi}}\sqrt{G_{\eta\eta}}}\frac{\partial\left((d+\zeta)V\sqrt{G_{\xi\xi}}\right)}{\partial\eta}=(d+\zeta)Q \tag{1}$$

$$\frac{\partial u}{\partial t}+\frac{u}{\sqrt{G_{\xi\xi}}}\frac{\partial u}{\partial\xi}+\frac{v}{\sqrt{G_{\eta\eta}}}\frac{\partial u}{\partial\eta}+\frac{\omega}{d+\zeta}\frac{\partial u}{\partial\sigma}-\frac{v^2}{\sqrt{G_{\xi\xi}}\sqrt{G_{\eta\eta}}}\frac{\partial\sqrt{G_{\eta\eta}}}{\partial\xi}+\frac{uv}{\sqrt{G_{\xi\xi}}\sqrt{G_{\eta\eta}}}\frac{\partial\sqrt{G_{\xi\xi}}}{\partial\eta}-fv=-\frac{1}{\rho_0\sqrt{G_{\xi\xi}}}P_\xi+F_\xi+\frac{1}{(d+\zeta)^2}\frac{\partial}{\partial\sigma}\left(\nu_V\frac{\partial u}{\partial\sigma}\right)+M_\xi \tag{2}$$

$$\frac{\partial v}{\partial t}+\frac{u}{\sqrt{G_{\xi\xi}}}\frac{\partial v}{\partial\xi}+\frac{v}{\sqrt{G_{\eta\eta}}}\frac{\partial v}{\partial\eta}+\frac{\omega}{d+\zeta}\frac{\partial v}{\partial\sigma}-\frac{u^2}{\sqrt{G_{\xi\xi}}\sqrt{G_{\eta\eta}}}\frac{\partial\sqrt{G_{\xi\xi}}}{\partial\eta}+\frac{uv}{\sqrt{G_{\xi\xi}}\sqrt{G_{\eta\eta}}}\frac{\partial\sqrt{G_{\eta\eta}}}{\partial\xi}-fu=-\frac{1}{\rho_0\sqrt{G_{\eta\eta}}}P_\eta+F_\eta+\frac{1}{(d+\zeta)^2}\frac{\partial}{\partial\sigma}\left(\nu_V\frac{\partial v}{\partial\sigma}\right)+M_\eta \tag{3}$$

Where, ζ is the water level above the reference level in m, t is the time in s, $\sqrt{G_{\xi\xi}}$ and $\sqrt{G_{\eta\eta}}$ are coefficients used to transform curvilinear to rectangular coordinates in m, d is the depth below the reference level in m, U is the depth−averaged velocity in the ξ−direction in m/s, V is the depth−averaged velocity in the η−direction in m/s, ξ and η are the cartesian orthogonal curvilinear coordinates used by Delft3D in the horizontal directions and, Q is the global source or sink per unit area in m/s, u is the flow velocity in the ξ−direction in m/s, v is the flow velocity in the η−direction in m/s, ω is the vertical velocity component in m/s, σ is the scaled vertical coordinate, $\sigma=\frac{z-\zeta}{d-\zeta}$, f is the Coriolis parameter (inertial frequency) in s^{-1}, ρ_0 is the reference density of water in kg/m^3, P_ξ is the gradient hydrostatic pressure in the ξ−direction in $kg/(m^2s^2)$, P_η is the gradient hydrostatic pressure in the η−direction in $kg/(m^2s^2)$, F_ξ is the turbulent momentum flux in the ξ−direction in m/s^2, F_η is the gradient hydrostatic pressure in the η−direction in m/s^2, ν_V is the vertical eddy viscosity, M_ξ is the source or sink of momentum in the ξ−direction in m/s^2, M_η is the source or sink of momentum in the η-direction in m/s^2.

When taken into account the effect of flow on the waves (via set-up, current refraction, and enhanced bottom friction) and the effect of waves on current (via forcing, enhanced turbulence, and enhanced bed shear stress), it is recommended to use an online coupling of Delft3D-WAVE with Delft3D-FLOW: the WAVE model has a dynamic interaction with the FLOW module of Delft3D (i.e. two way wave-current interaction). Through this coupling, both the effect of waves on current and the effect of flow on waves are accounted. SWAN estimates wave characteristics by the application of the spectral action balance (Eq. (3)) (Delft University of Technology, 2006):

$$\frac{\partial N}{\partial t}+\frac{\partial c_x N}{\partial x}+\frac{\partial c_y N}{\partial y}+\frac{\partial c_\sigma N}{\partial \sigma}+\frac{\partial c_\theta N}{\partial \theta}=\frac{S_{tot}}{\sigma} \quad (4)$$

Where, $\frac{\partial N}{\partial t}$ represents the local rate of change of action density in time, $\frac{\partial c_x N}{\partial x}$ and $\frac{\partial c_y N}{\partial y}$ represent propagation of action in geographical space, $\frac{\partial c_\sigma N}{\partial \sigma}$ represents shifting of the relative frequency due to variations in depths and currents, $\frac{\partial c_\theta N}{\partial \theta}$ represents depth-induced and current induced refraction $\frac{S_{tot}}{\sigma}$, c_x is the propagation velocity of the wave energy in the $x$direction of the (x,y) spatial space, $c_y$is the propagation velocity of the wave energy in the y direction of the (x,y) spatial space, c_σ and c_θ is the propagation velocity in the (σ,θ) spectral space and and S_{tot} is the source/sink term representing all the physical processes that dissipate, redistribute, or generate wave energy (Deltares, 2022b).

The model can be used to obtain realistic estimates of wave parameters in coastal and near-shore areas given certain conditions of wind, tides, SL, coastal circulation, and bed load changes; through the simulation of random waves generated by winds, representing the physical phenomena of wave propagation in time and space like shoaling, refraction, frequency change, wave generation by wind, non-linear wave-wave interaction, white-capping, bottom friction, depth-induced breaking and blocking of waves by current (Sun et al., 2022). SWAN plus FLOW in Delft3D assesses two-dimensional (2D) coastal hazard parameters such as tidal range through water elevation, H_s, mean wave period, and depth-averaged velocity around El Morro and Tumaco islands.

The model grid is created using the Delft3D Dashboard MATLAB v8.2 toolkit and the DELFT-3D-GRID module. The former facilitates grid generation around the islands and incorporates a 30° rotation to align with Tumaco Bay's geometry, enhancing the efficiency of the results, while the latter complements the grid at points near the coast. These tools are selected for their flexibility in managing complex geometries, generating networks, and extracting tide components from the TPXO-8 model for each imposed boundary condition. A uniform grid resolution of 100 m is chosen, balancing computational efficiency with the resolution required to capture essential hydrodynamic features within the study area. The uniformity of the grid resolution and the aspect ratio of 1 are intentionally maintained to provide a consistent representation of physical processes across the simulation domain.

To assess the robustness of the FLOW model in Tumaco Bay and the results' independence from the computational domain resolution constructed, grid independence tests are conducted using various structured grids with resolutions of 25 m, 50 m, 100 m, and 200 m. An independence-grid test is executed, utilizing 15 randomly selected observation points. These points undergo two open ocean boundary conditions, informed by astronomical components generated in the TPXO8 global tidal model available in the DelftDashboard tool, and with a boundary of the water level from the data measured by the Dimar tidal gauge. The calibration period lasts 4 days, performed on an hourly basis.

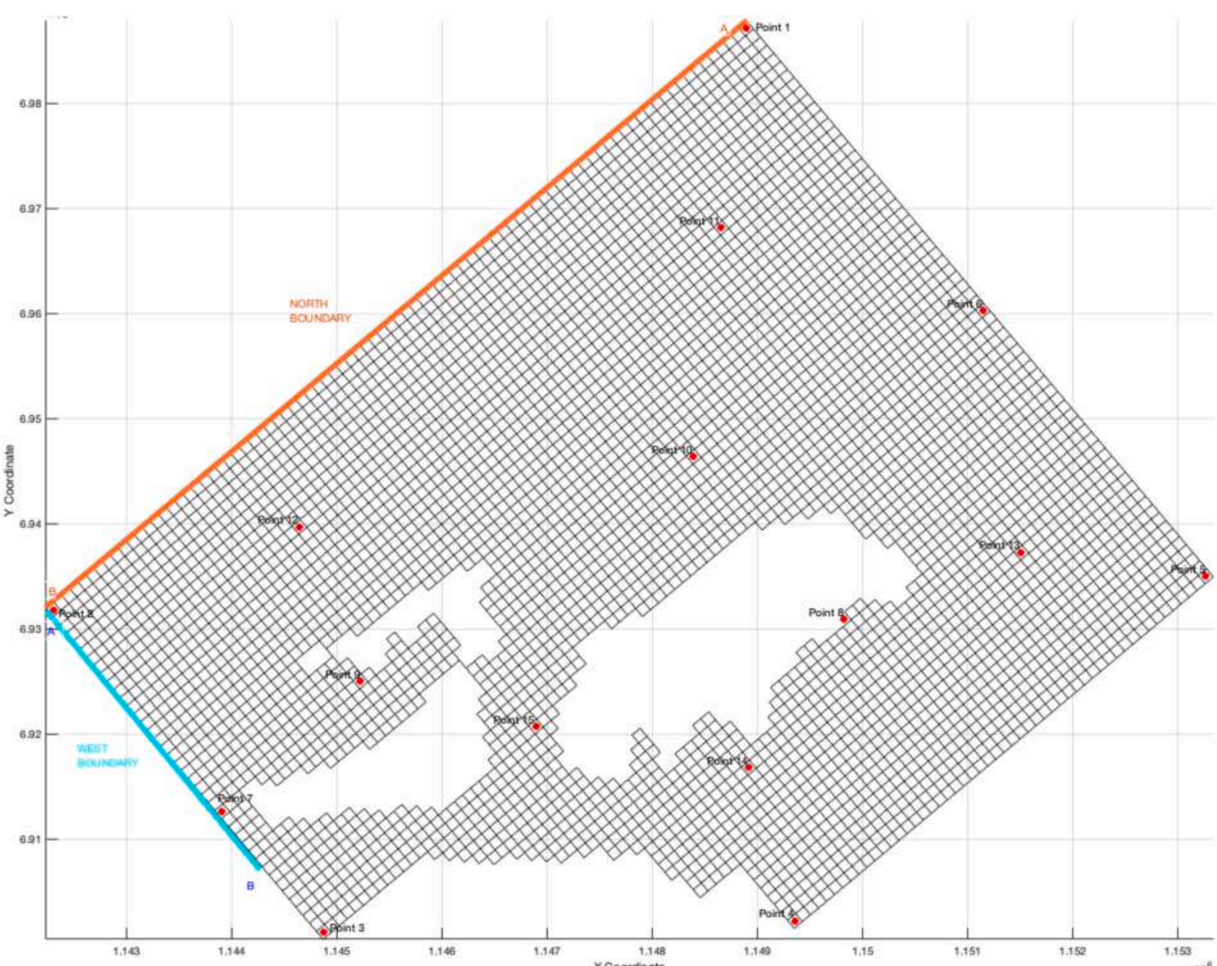

Fig. 3. Random points location and TPXO8 Boundary Conditions in the computational domain.

The choice of mesh is guided by its capability to accurately represent the mesotidal process in Tumaco Bay, as observed around the 15 selected points concerning the tidal phenomenon, with the values approaching the MSL of 1.61 m and its recurrence. Fig. 3 shows the locations of random points in the 100 m computational domain.

After establishing the grid, the Delft3D-QUICKIN module is utilized to integrate bathymetric data into the established grid. This module implements a grid cell averaging interpolation method, which computes the average depth for each grid cell by considering all available bathymetric data points within that cell's boundaries. This approach is effective for areas with gradual depth changes and where bathymetric data points are distributed irregularly.

Prior to deploying the WAVE module, the hydrodynamic model was calibrated and applied within the Delft3D-FLOW. This phase used hourly SL data from July 2017 to July 2018 and wind data recorded every six hours over the same period. A time step of 0.2 min was selected to ensure the stability of the model under the initial conditions, which included a water level of 2.69 m corresponding to the observed SL in Tumaco, salinity of 33 ppt, and a temperature of 24 °C. Three boundary conditions were configured from the north, west, and south, with the first two representing the open ocean limit conditions. These define the external forcing and act as the initial wave field for the simulation. The TPXO8 global tidal model was integrated to account for tidal forcing, known for its comprehensive global coverage and high accuracy in predicting tidal constituents, providing values for each of the imposed conditions. The southern boundary condition was informed by hourly SL data measured by DIMAR's tide gauge.

Astronomical tidal forcing is imposed along the open-ocean boundaries of the model domain using harmonic constituents from the TPXO8 global tidal model (DelftDashboard extraction, 1/8° resolution), widely applied in coastal studies with limited in situ data. During calibration, the modeled MSL is adjusted to 1.61 m (A0 feature) and a phase offset of 0° is confirmed for the M2 constituent to align simulated water levels with observations from the DIMAR Tumaco tide gauge, which is used for model validation.We use the cyclic advection scheme for momentum in Delft3D-FLOW. This internal numerical method for discretizing horizontal advection is selected because it conserves mass and momentum and reduces artificial reflections in strongly oscillatory tidal environments (De Goede, 2020) such as Tumaco Bay. Short sensitivity tests show that this configuration yields stable tidal propagation and good agreement with observed water levels at our 100-m grid resolution.

Following the hydrodynamic setup, the WAVE module of Delft3D was executed in line with the FLOW module. The spectral resolution for wave modeling was set at a minimum frequency of 0.05 Hz and a maximum of 1 Hz, spanning 36 directions to capture a comprehensive range of wave phenomena. Boundary conditions were derived from uniform conditions from two directions: Northeast, and Northwest. These were informed by measured data from DIMAR's wave buoy, which recorded maximum H_s of 1.6 m and peak periods of 25 s.

For the physical parameters, the JONSWAP spectrum was utilized with a bottom coefficient of 0.067 m^2/s^3 to describe the wave energy distribution. The JONSWAP spectrum is often selected in coastal engineering studies because it is well-suited for simulating growing sea conditions where wind input is significant (Vledder et al., 2011). A Non-stationary computational mode was chosen for the simulation with a coupling interval of 60 min and a time-step of 20 min (Vledder et al., 2011).

The online coupling capability of Delft3D seamlessly integrates the hydrodynamic FLOW module with the WAVE module (SWAN), permitting the direct incorporation of hydrodynamic simulation results from FLOW into WAVE module calculations. Operating these modules concurrently allows the model to ensure that wave transformations are informed by and exert influence on the current velocities and water levels and vice versa.

2.4. Coastsat application

CoastSat provides a set of tools for monitoring and exploring coastlines. The software is freely available on GitHub (https://github.com/kvos/CoastSat) (Tamiminia et al., 2020). The temporal resolution of the shoreline provided by CoastSat is approximately biweekly, with a horizontal accuracy of 10 m to 30 m on any sandy coast worldwide. However, biases introduced by tides should also be considered. These biases arise from sensors synchronized with the sun that only sample fixed combinations of diurnal/semidiurnal and neap-spring tidal cycles, which can result in aliasing (a phenomenon that occurs in the representation of digital signals or images when the frequency of the original signal is insufficiently sampled). To correct this bias, it is recommended that along coastlines with large tidal ranges and/or flatter beach profiles, all shorelines be adjusted to a standard reference elevation. For the mesotidal environment of the Tumaco-Nariño study area, each image is acquired at different tidal stages, so a linear tidal correction is applied using measured water levels and the characteristic slope of the beach face to translate each shoreline to a reference elevation as follows:

$$\Delta x = \frac{z_{ref} - z_{wl}}{m}$$

Where Δx is the transverse horizontal displacement along the transects normal to the coast, z_{ref} is the reference elevation (e.g., 0 m above MSL), z_{wl} is the local water level (tide + residual) at the time of image acquisition, and m is a characteristic slope of the beach face. The precise time of image acquisition to obtain the local water level is stored in the image metadata.

2.5. Correlation analysis of variables with ShoreLine displacement (SLD)

In this section, we analyze the correlation between the reanalysis data from Waverys, and the SLD of the El Bajito and El Morro beaches obtained with CoastSat. Data from 1993 to 2018, with a three-hour timestep, are utilized, focusing on H_s, T_p, Θm, as well as Stokes drift velocities (SDX and SDY), Mean Wave Period (MT_p), Wind Wave Direction (WWD), Wind Wave Significant Height (H_s_WW, representing the significant height of the locally generated wind sea), Wave Direction at Variance Spectral Density Maximum (WVP), and SL). The level of influence and significance of these variables on SLD is identified using a RF.

RF helps to analyze the contribution of each variable to the changes observed in the SLD. The model's primary advantage is its ability to handle a large number of variables simultaneously, identifying the most important ones while accounting for complex interactions between them (Enríquez-Hidalgo et al., 2022; Siders and Keenan, 2020). The model allows us to discover patterns that are not readily apparent in linear correlation analyses, making it ideal for coastal studies where nonlinear interactions between environmental factors play a significant role (Garge et al., 2013).

The method is selected for this analysis due to its robustness in handling high-dimensional datasets, as well as its capacity to provide interpretable results through feature importance scores. Unlike other ML models, RF works well with both categorical and continuous variables, making it a versatile choice for the wide range of physical oceanographic variables (Fogarin et al., 2023). Additionally, its resistance to overfitting makes it particularly useful when working with environmental data that can be sparse or contain noise (Arjasakusuma et al., 2021).

RF operates by constructing an ensemble of decision trees during the training phase, where each tree is generated using a randomly selected subset of the data; the output of the model is the mean prediction from all trees (Genuer et al., 2015). For this study, we use the randomForest package in R to build the RF model (Garge et al., 2013). The input variables are the environmental factors mentioned earlier, and the target variable is the observed SLD over time. Each tree within the model analyzes a different combination of the variables, allowing the model to learn complex, nonlinear interactions that influence SLD. The importance scores for each variable are calculated using the *mean decrease in Gini impurity*, which indicates how much the variable improves the model's ability to classify or predict the target variable (Siders and Keenan, 2020). The importance of each feature is computed as the average decrease in impurity (e.g., Gini impurity or mean squared error) across all trees in the forest. The formula for calculating the feature importance *FI* in RF is:

$$FI(j) = \frac{1}{T}\sum_{t=1}^{T}\left(I_t - I_t^{(j)}\right)$$

where $FI(j)$ is the importance of feature j, T is the total number of trees, I_t is the total impurity of the tree, and $I_t^{(i)}$ is the impurity of the tree if the splits on feature j were not allowed (Siders and Keenan, 2020).

Two RMSE values were compared: the Out of Bag (OOB) error, which uses randomly selected subsets of data not included in the training of each individual tree (bootstrap aggregation), and the test error, calculated using 70 % of the data for calibration and the remaining 30 % for validation. The observed similarity between these two errors indicates that these configurations strike an optimal balance between computational efficiency and predictive accuracy for both study areas. Additionally, the mtry parameter, which controls the number of variables randomly selected at each split, was set to 6 for El Bajito and 4 for El Morro, further optimizing the model's performance.

For the calibration and validation of the RF models, the algorithm was initially configured with 1500 regression trees. However, it was determined that 1344 trees for El Bajito and 1291 trees for El Morro provide the lowest test RMSE values, achieving 10.94 m for El Bajito and 9.21 m for El Morro, as illustrated in Fig. 4. The magnitude of the error is attributed to the spatial resolution of the Landsat images used, with a 30 m resolution between each shoreline line over time, which limits the precision in tracking SLD. However, the RMSE values obtained in this study are consistent with those reported in the literature, such as Billet et al. (2024), who found RMSEs between 3.8 m and 10.2 m when comparing satellite data with in-field measurements.

Two RMSE values were compared: the Out of Bag (OOB) error, which uses randomly selected subsets of data not included in the training of each individual tree (bootstrap aggregation), and the test error, calculated using 70 % of the data for calibration and the remaining 30 % for validation. The observed similarity between these two errors indicates that these configurations strike an optimal balance between computational efficiency and predictive accuracy for both study areas. Additionally, the mtry parameter, which controls the number of variables randomly selected at each split, was set to 6 for El Bajito and 4 for El Morro, further optimizing the model's performance.

3. Results and discussion

In this study, a multidisciplinary new approach is employed to analyze SLD patterns on the beaches of Tumaco, Colombia, using various tools. Initially, the hydrodynamic model FLOW, coupled with the wave model SWAN within the Delft3D software, is applied to simulate hydrodynamic and wave conditions in the study region. Subsequently, the CoastSat tool is used to obtain the SLD in different beach transects. Finally, a RF model is implemented to identify the most important physical variables influencing shoreline changes, using the results from SWAN, FLOW, and the Waverys reanalysis data as inputs, and SLD as the response variable. The key findings from each of these stages are discussed below, and our results are compared with previous studies on hydrodynamics, waves, erosion, and accretion in other regions of the world.

3.1. FLOW calibration and validation and SWAN comparison

Fig. 5 depicts the water level results (in meters) over a four-day simulation period. The 100 m grid is found to best capture the recurrence conditions, matching both the mean water level defined in the boundary conditions and the tidal oscillations observed in the mesotidal environment around Tumaco and El Morro Islands. In addition, it achieves this with a significantly lower computational cost compared to the 50 m and 25 m grids, while showing a maximum water level difference of 5 cm relative to the finer grids. This result indicates that the model outcomes are independent of the grid spatial resolution. Therefore, for practical reasons and superior performance, the 100 m grid is selected for subsequent calibration steps.

In Fig. 6, a time series for the total duration of simulations shows water level data from 2017 to 2018 (6a), with a zoomed-in view of the month of June (6b), highlighting the model's underestimation. Fig. 6c presents a scatter plot that shows the correlation between observed and simulated water levels, supported by a correlation coefficient of 0.98, a Root Mean Square Error (RMSE) of 4 cm, and a bias of −0.5 cm, indicating that the model tends to slightly underestimate the observed values.

Regarding the calibration, validation and comparison of the FLOW and SWAN results, studies such as those by Martos and Isabel (2022) indicate that RMSE of 6 to 8 cm and correlation coefficients of 0.7 to 0.8 are obtained when comparing measured and simulated water levels using the global tide model TPXO8 as boundary conditions for their model and comparing with in situ tide gauges around the Gulf of Cádiz, where the Atlantic Ocean connects with the Mediterranean Sea. Despite the existence of the TPXO9 model, the authors point out that this newer model is not always the best option for use in FLOW. In our study, an RMSE of 12.8 cm and a correlation coefficient of 0.9 were achieved. This

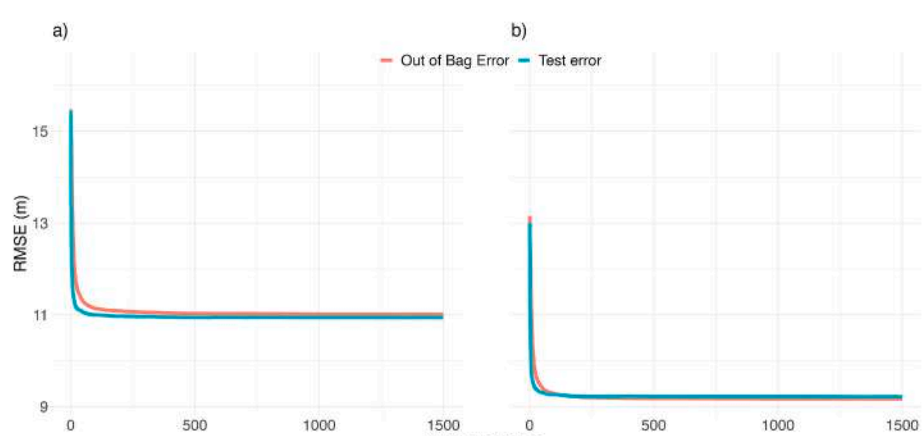

Fig. 4. Random Forest RMSE Calibration a) Bajito Beach and b) El Morro Beach.

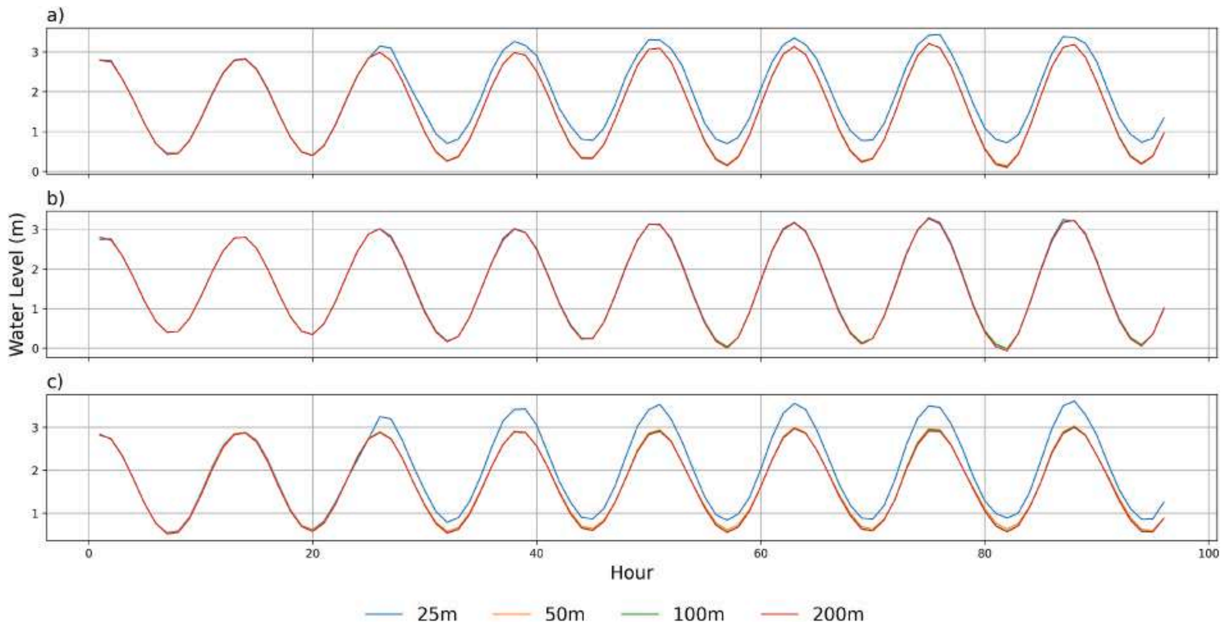

Fig. 5. Water level in random points around Tumaco and El Morro Islands a) random point 10, b) random point 12 and c) Random point 13.

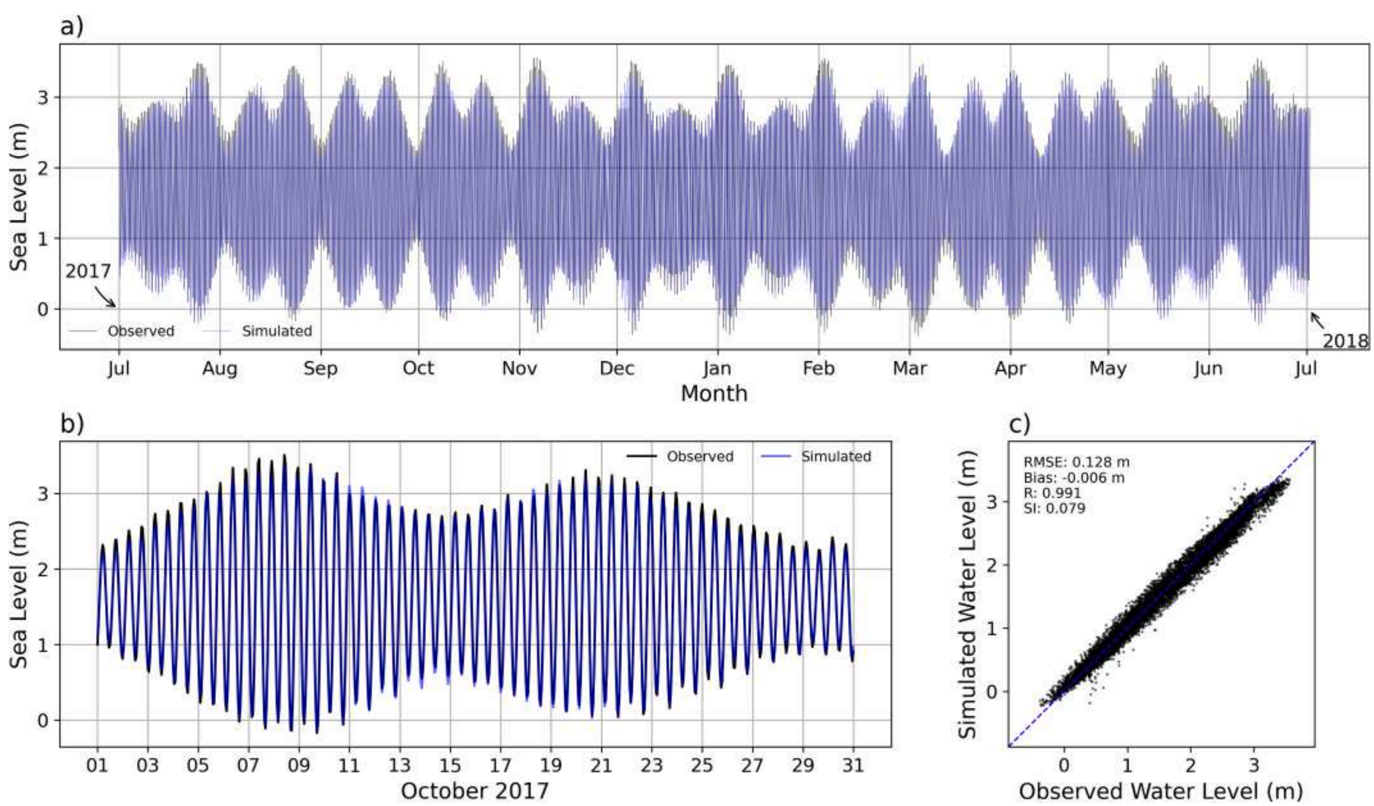

Fig. 6. Observed vs simulated water level data. a) Water Level 2017–2018, b) Water Level October 2018 and c) Scatter Plot Water Level.

improvement in correlation can be attributed to the coupling of the FLOW and SWAN modules and the inclusion of winds. The authors suggest that these additional improvements enhance the model's precision in Delft3D, as evidenced in this research.

Additionally, Law et al. (2023) found that the reanalysis data from Waverys were validated with wave buoy observations and compared with ERA5 data, highlighting that the scatter index maps show very good performance for Waverys, with an index below 9 % at mid- and intermediate latitudes. The scatter index increases to a range between 12 % and 16 % in coastal ocean areas and enclosed seas. The low scatter index values found in the open ocean for both reanalysis systems cover more domains in Waverys than in ERA5. Regarding the tropics (location of the study area), the H_s from Waverys shows an overestimation of 20 cm with a mean standard deviation of 0.24 m compared to in-situ buoys for the period 1994–2015. Similarly, the T_p in the tropics has a difference of −0.38 s and a mean standard deviation of 0.69 s. For Θm, the mean standard deviation is 37.15° with a mean difference of 1.98°(Law et al., 2023).

Additionally, Fig. 7 presents the results of H_s, T_p and Θm comparing the data modeled with SWAN and the reanalysis data from the Copernicus Marine Service using the Waverys product. In this figure, 7a and 7b represent the time series of observed and simulated H_s and T_p, respectively. 7c and 7d shows the observed and simulated Θm along with the magnitudes of H_s. It is noted that for H_s, the model shows an underestimation of 1.6 cm; for the T_p, an underestimation of 0.67 s; and for the Θm, an overestimation of 1.2°.

When considering H_s, T_p, and Θm, in situ measurements are generally the most reliable data. However, these measurements are very limited in terms of time and space. There are also temporal gaps in these data due to extreme storms, and some of the data have been affected by refraction, local winds, and sandbank formation. The number of available instrumental records is far from what is needed to adequately model wave-related processes, especially in developing countries including Tumaco-Nariño. Therefore, it is necessary to use reanalysis data and numerical models that can cover larger areas and longer time periods (Juan et al., 2024).

Our comparison between SWAN simulations and Waverys reanalysis at Tumaco indicates modest bias and low error for significant wave height (RMSE ~0.05 m; bias ~ − 0.05 m), with higher errors for T_p (RMSE ~1.6 s) and small Θm differences (RMSE ~6–7°) but strong correlation across all metrics ($R \geq 0.96$). These values are broadly consistent with ranges reported in regional and global reanalysis comparisons where in situ observations are sparse or intermittent. For example, Espinoza Villacís et al. (2023) compare Delft3D wave

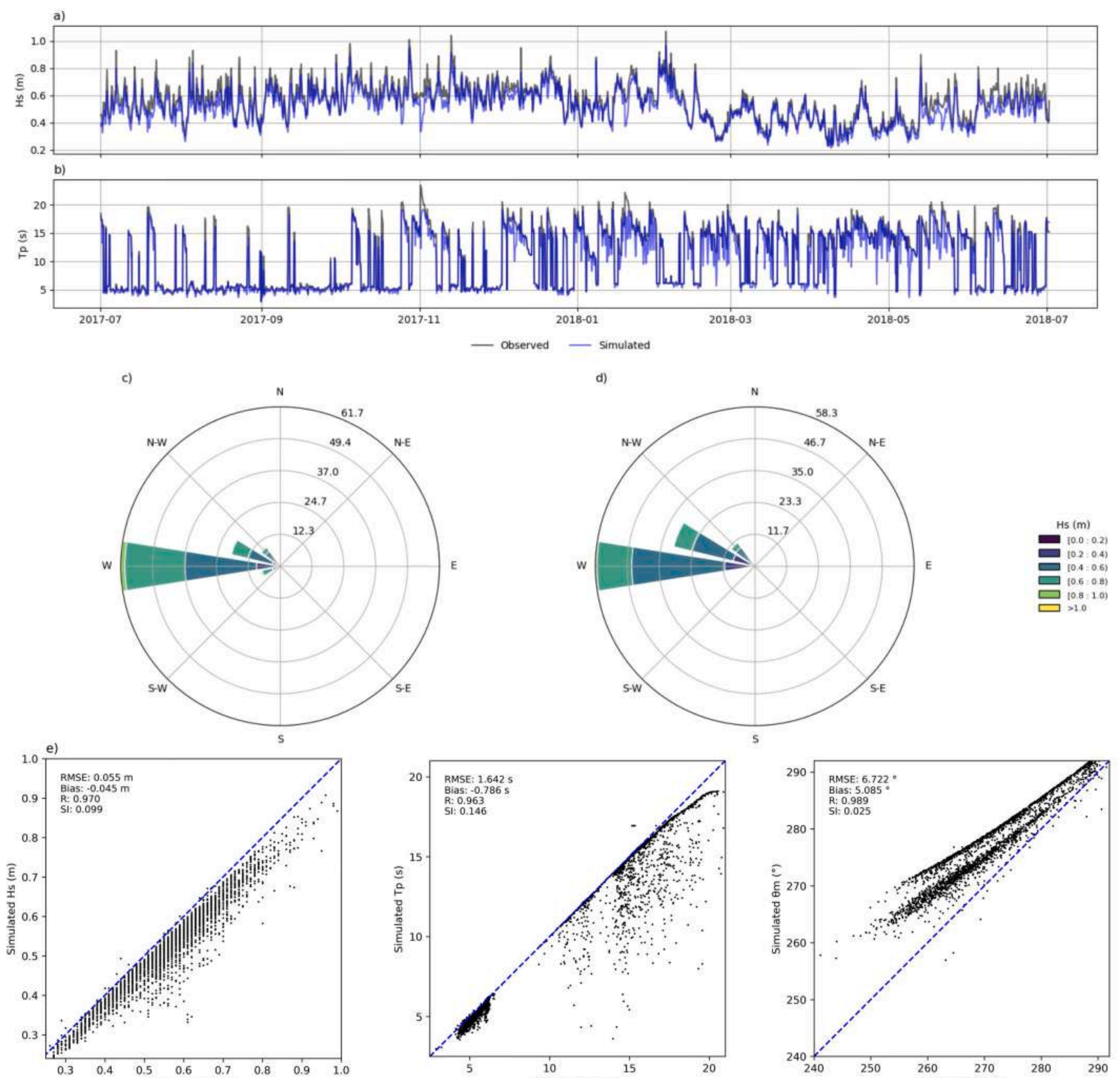

Fig. 7. Observed vs simulated wave parameters a) Significant Wave Height (H_s), b) Peak Wave Period (T_p), c) Observed Wave Direction (O-Θm), d) Simulated Wave Direction (S-Θm) and e) Scatter plots of observed vs simulated H_s, T_p and Θm.

modeling with Waverys virtual points along the Ecuadorian Pacific and report low H_s errors (RMSE 0.03–0.04 m) and directional agreement similar to ours. Studies in Central America also use Waverys where buoy coverage is limited; Alfaro-Chavarría et al. (2023) report RMSE spans of 0.21–0.55 m for H_s and 0.96–4.5 s for T_p across Costa Rican Pacific and Caribbean sites, illustrating the variability inherent in mixed coastal settings with heterogeneous data quality. Law et al. (2023) further show that Waverys tends to underestimate H_s in tropical regions, which is consistent with the small negative bias in our results.

Broader multi-buoy assessments reinforce that reanalysis products can provide useful wave climatologies when carefully interpreted. Wang and Wang (2022) compare buoy observations across U.S. Atlantic and Pacific coasts with ERA-class wave reanalyses and document seasonal skill variability in H_s and T_p comparable to the spread we observe

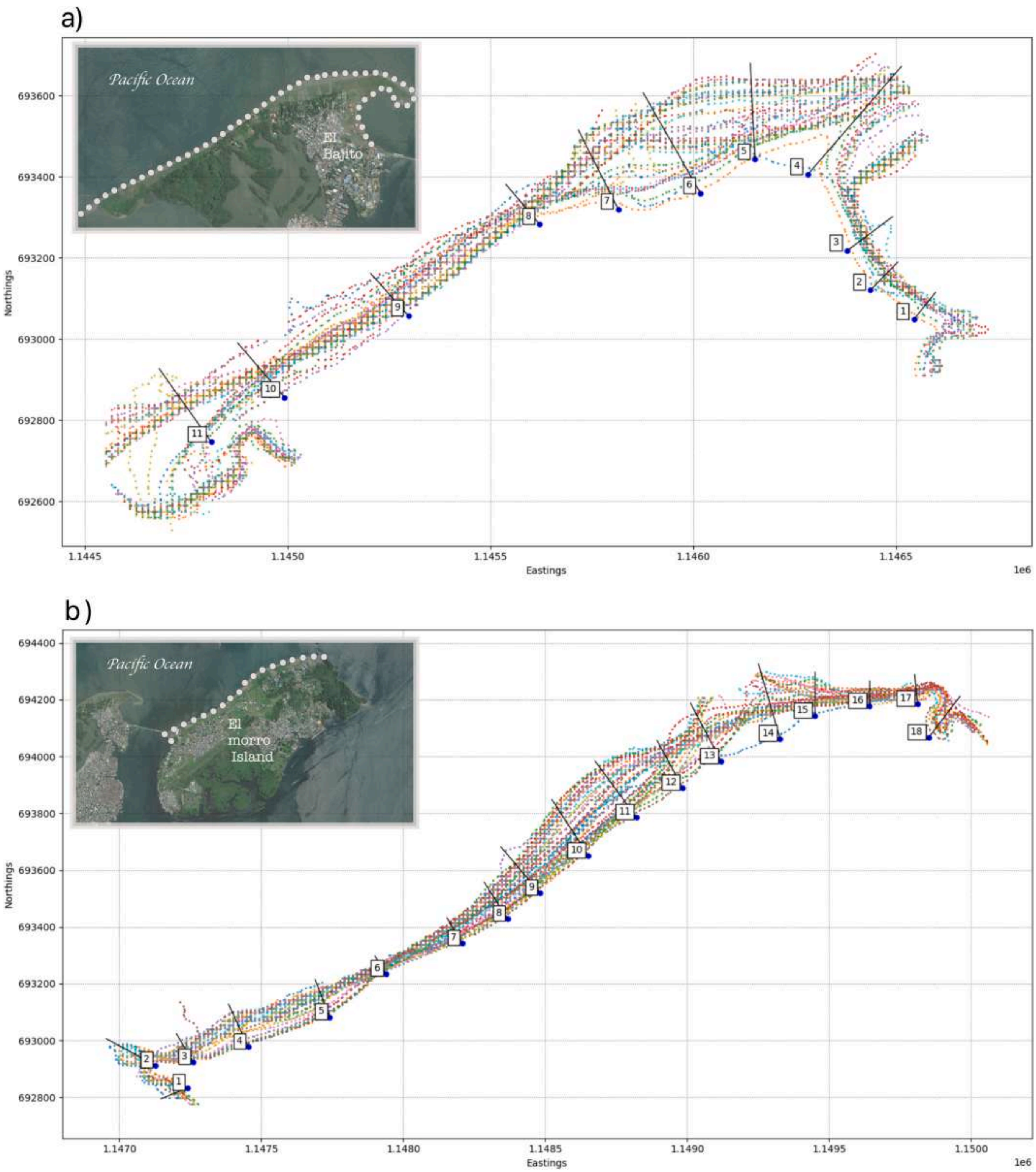

Fig. 8. Shorelines at Morro Beach (A) and El Bajito Beach (B) from 1993 to 2024.

relative to Waverys. In semi-enclosed basins, Juan et al. (2024) report higher RMSEs for T_p and Θm when comparing Mediterranean buoys with Waverys, highlighting that complex local bathymetry can degrade performance an issue relevant to Tumaco's estuarine geometry. Taken together, these studies support our use of Waverys as an external reference dataset for evaluating modeled wave conditions in the Colombian Pacific, where long, continuous, high-confidence buoy records are not available.

While differences across studies underscore that long, high-quality buoy records provide the strongest validation, our results—together with published comparisons show that reanalysis products such as Waverys can serve as a practical alternative where real-time buoy data are sparse. This is particularly relevant for data-limited coasts in Colombia and neighboring Ecuador. Moreover, the error magnitudes reported here are small relative to the observed variability of the local wave climate, making these data suitable for exploring the influence of wave forcing on SLD in Tumaco and similar settings.

3.2. ShoreLine displacement (SLD)

The SLD of El Bajito Beach and Morro Beach were obtained from January 1, 1993, to May 5, 2024 (31 years), using Landsat 5, 6, 7, 8, and 9. After selecting and filtering the data, 43 shoreline lines were processed for bajito Beach (Fig. 8a) and 55 shoreline lines for El Morro Beach (Fig. 8b). Additionally, Figs. 9 and 10 shows the trend slopes diagrams for each beach, and the SLD evolution whit monthly average in two times of the total period (1993–2024) for El Bajito beach and Morro Beach Respectlily.

Fig. 9 shows the bar charts for the 11 transects of El Bajito beach, which has an approximate length of 2.5 km. In the first analysis period (1993–2005), transect 4 exhibits accretion with a rate of 34.32 m/year, while transect 9 shows erosion at −7.84 m/year. In the second period (2014–2024), the variability between the transects decreases, although patterns of erosion and accretion persist. Three key transects are highlighted: transect 3, which transitions from erosion in the first period to accretion in the second (yellow color); transect 5, which shows consistent accretion across both periods (blue color); and transect 9, which experiences sustained erosion in both periods of analysis (red color).

Transect 3 shows a notable shift in behavior. During the first period (1993–2005), it exhibits a clear erosional trend, whereas in the second period (2014–2024), the trend shifts to accretion. This change may be associated with beach recovery due to hydrodynamic conditions, particularly sediment supply from the Mira River and wave forcing from the west of Tumaco Island, which more strongly impacts the southwestern part of the island where transects 8 to 11 are located. These transects show consistent erosion across both periods.

In contrast, transects 1 to 7, located further northeast, generally show accretion, especially in the most recent period. This behavior may be attributed to the formation of a sediment bar in the northeastern part of Tumaco Island, which acts as a coastal barrier, providing greater protection to the inner area and the eastern part of El Bajito beach.

Fig. 10 shows SLD at El Morro Beach with a l length of 3.5 km over two periods: 1993–2000 and 2001–2024. In the first period, there is greater variability across the transects, with transect 14 showing the highest accretion rate (30.67 m/year) and transect 10 showing the highest erosion rate (−13.52 m/year). This variability decreases in the second period, where the trends are more stabilized. Notably, transects 1 to 11 show a general trend towards accretion, likely due to the natural protection provided by Tumaco Island and a sandbank that extends to 1.83° latitude and − 78.74° longitude. Transect 5 (blue color) shows a consistent accretion trend across both periods, which may be related to its location, protected by the barrier island. Additionally, this sandbank aligns longitudinally with transect 11 (red color), which shows significant erosion in the first period, followed by stabilization in the second. The location of this transect, near the edge of the sandbank, suggests that the reduction in erosion may be due to increased sediment accumulation in recent years.

For transects 12 to 15, a change in the beach's orientation is observed, along with direct exposure to open water, creating conditions more favorable to erosion. This exposure to wave action from the

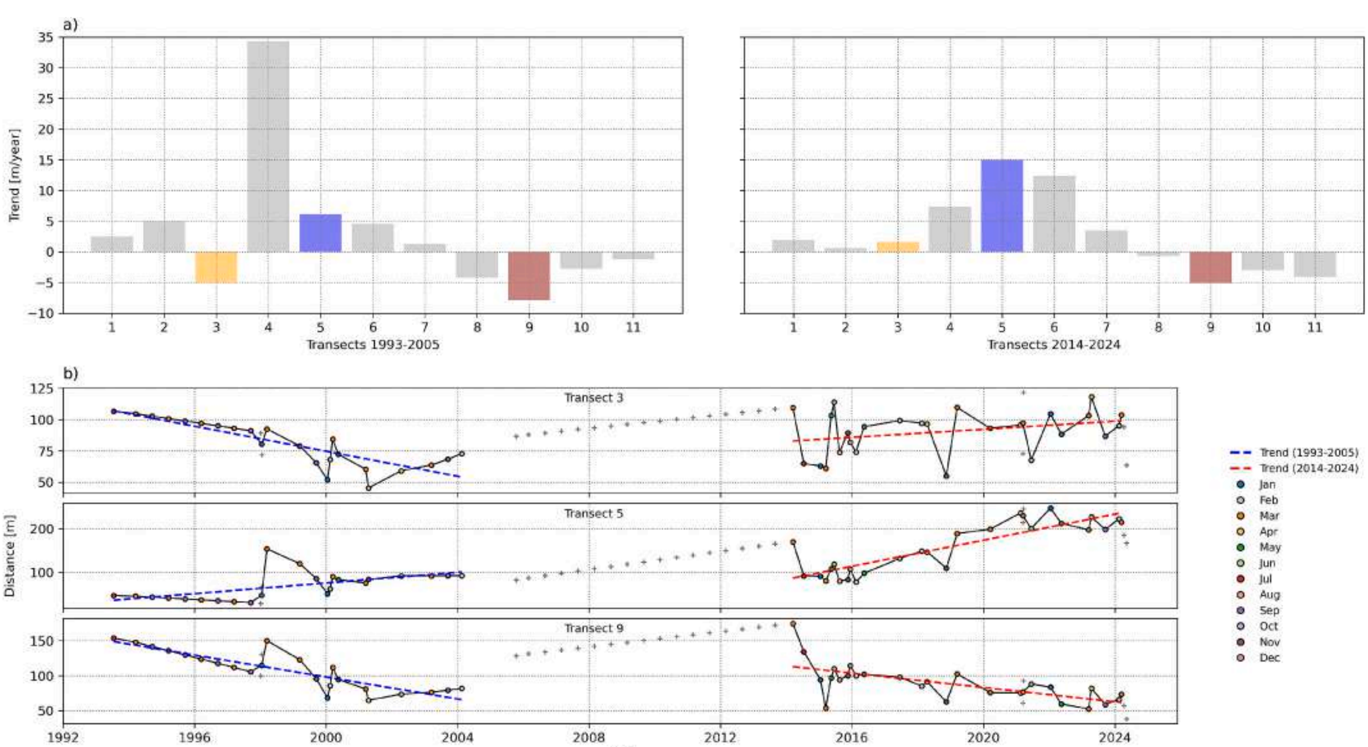

Fig. 9. El Bajito Beach SLD a) Trend slopes for SLD across transects 1 to 11 during the periods 1993–2005 and 2014–2024. b) Temporal variability of SLD for transects 3, 5, and 9, with monthly data points.

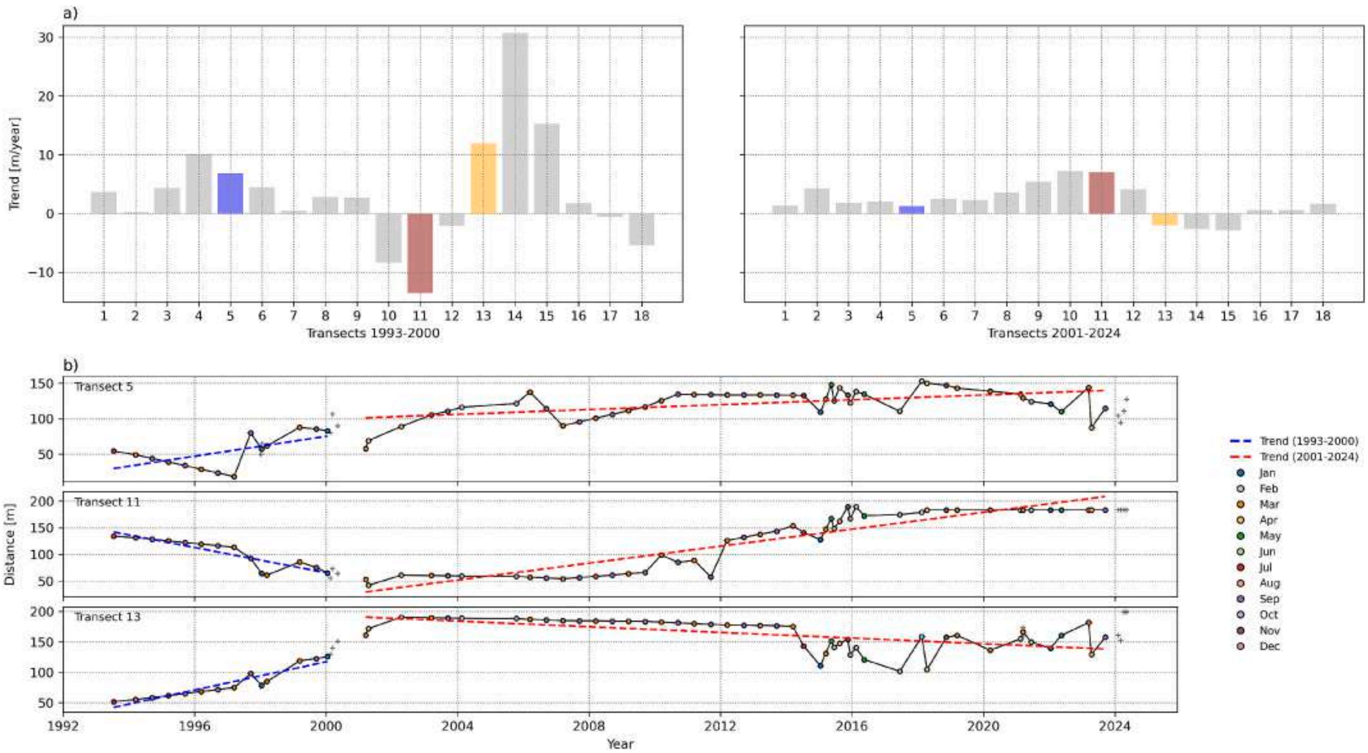

Fig. 10. El Morro Beach SLD a) Trend slopes for SLD across transects 1 to 18 during the periods 1993–2000 and 2001–2024. b) Temporal variability of SLD for transects 3, 5, and 9, with monthly data points.

northwest is likely a key factor in the erosive processes affecting this part of the beach, which is also one of the most important tourist areas in the region, home to Tumaco's main hotels and restaurants. This is particularly noticeable in transect 13 (yellow color), where a significant accretion trend is seen in the first period, followed by a slight erosive trend in the second period. This pattern suggests that the sediment accumulation from the Mira and Rosario rivers is no longer sufficient, and that coastal forcing is stronger in this part of the beach.

Transects 16 to 18 show a pattern of accretion, though of a lesser magnitude compared to transects 12 to 15. These transects, located in the northeastern corner of El Morro Island, may be receiving sediment deposits transported from the other transects in a west-to-east direction, partially compensating for the erosion observed in the transects more exposed to open water.

The analysis of SLD at El Morro and El Bajito beaches reflects the unique characteristics of an estuarine environment, with semidiurnal tides and a mesotidal range, which contrast with the results observed in previous studies conducted on open beaches. At El Morro and El Bajito, patterns of accretion and erosion were similar, with SLD ranging from 0 m to 200 m. These results differ significantly from those observed in Mar del Plata, Argentina, where open beaches measuring 1 to 1.5 km in length show linear SLD trends ranging from −0.6 to 0.7 m/year, with SLD varying between 7 m and 83 m. In that region, semidiurnal tides have an average amplitude of 0.78 m and a maximum of 1.63 m, influencing the sedimentation and coastal displacement patterns (Billet et al., 2024). Unlike Mar del Plata, at El Morro and El Bajito, the influence of rivers and the estuarine geomorphology, combined with the greater exposure of some transects to open water, generate more complex dynamics that vary considerably between different sectors of the beach.

Similarly, the results obtained on the Pacific coast of Mexico, specifically in Mazatlán, show an SLD range of between 0 m and 100 m in a semidiurnal tidal environment with a maximum amplitude of 1.8 m (Valderrama-Landeros et al., 2022). While the wave and tidal conditions in Mazatlán are comparable to those in Tumaco, the maximum SLD in Mazatlán are smaller than those observed at El Morro and El Bajito beaches. This difference can be partly explained by the estuarine characteristics of Tumaco, where the interaction between river currents, sediment supply from the Mira and Rosario rivers, and wave dynamics contribute to greater variability in the patterns of accretion and erosion.

Comparing these results with those of the coasts of Chile and Peru, where significant erosion is reported during El Niño events, especially the 1997/1998 event, notable differences are found (Vos et al., 2023). In Chile and Peru, approximately 50 % of the transects experienced erosion during El Niño events, whereas in Tumaco, the prevalence of accretion suggests a different coastal dynamic. It is possible that local factors, such as fluvial sedimentation or the specific geomorphological characteristics of Tumaco, play an important role in these observed patterns, influenced by sediment contributions from the Mira and Rosario rivers. Similarly, during La Niña phases, the coasts of Chile and Peru tend to show accretion, although not as pronounced as the erosion during El Niño. This pattern partially aligns with the results in Tumaco, where accretion is observed in most transects in both El Morro and Bajito. However, the magnitude of accretion in Tumaco appears to be greater, suggesting that sedimentary recovery mechanisms may be more effective or intense in this region(Vos et al., 2023).

In comparison with the coasts of the United States, where erosion during El Niño events affects between 54 % and 67 % of the transects, Tumaco shows relative resilience to these events. The erosion values in Tumaco, although present, do not reach the severity reported in the United States (Vos et al., 2023), indicating that coastal dynamics in Tumaco may be influenced by factors other than ENSO. Although generalized erosion in the Western Pacific during El Niño events is evident, the results in Tumaco do not reflect this trend uniformly. This discrepancy opens the discussion on local particularities that may be modulating the response of Tumaco beaches to global climatic events.

An important point to emphasize, in line with previous studies, is that SLD analysis should not focus solely on the position of the shoreline, but also on the volumes of sediment being transported within the coastal zone (Valderrama-Landeros et al., 2022; Billet et al., 2024). The SLD may serve as an indirect indicator, but it is the volume of sediment being transported and deposited that ultimately determines the processes of erosion and accretion on a beach. In this sense, the estuarine beaches of Tumaco present a distinct context, where tides and river sediment supply differentiate them from the open beaches analyzed in Argentina and Mexico.

3.3. Random forest (RF) analysis of hydrodynamic and wave impact on Shoreline Displacement (SLD)

The Waverys Data, comprising various oceanographic parameters, offer valuable insights into coastal forcing. Specifically, H_s is a critical factor; values exceeding 1.1 m indicate a significant potential to affect the shoreline, while values less than 0.2 m suggest minimal impact (Mullick et al., 2019). In this research, H_s values remained primarily below 1 m, indicating moderate to low wave conditions that may not be sufficient to cause marked erosion, as observed with CoastSat tooktik (chapter 3.2). Tidal range also influences SLD dynamics. In this case, the tidal range is mesotidal, ranging between 2 and 4 m, suggesting a moderate influence on coastal erosion and sedimentation (Pramanik et al., 2019).

Although T_p data require further validation to confirm their effects on SLD, some preliminary implications can be inferred (Castelle et al., 2016) that wave periods reflect the energy and momentum of waves; longer periods could result in waves reaching farther inland during storm events, impacting flood extents. Conversely, shorter periods might be associated with higher wave frequencies, contributing to chronic erosion and altering sediment transport dynamics along coastlines (Pollard et al., 2019). In this study, T_p remained within moderate ranges, suggesting a limited influence on coastal erosion.

The importance of the variables for the RF model at El Bajito and El Morro beaches is closely related to the hydrodynamic and wave conditions of the area (see Table 1). Analyzing Fig. 7, it is observed that the H_s range between 0.4 m and 1.0 m, indicating relatively minimal wave action. SL emerges as the most important variable in the model, which aligns with the mesotidal range of Tumaco, where Fig. 6 shows a variation of up to 1.6 m. Fluctuations in SL directly impact coastal dynamics, especially in an estuarine environment like El Bajito and El Morro, where tidal variations can significantly influence shoreline erosion and accretion.

Θm and wind wave direction (WWD) also hold high importance in the model. Fig. 7c shows that the predominant Θm is towards the west, with a recurrence of 61 %. This directional pattern is crucial, as the orientation of the beach and exposure to waves coming from the west affect sediment transport processes and, consequently, the configuration of the SLD. The high influence of Θm in the model reflects how these waves, despite their moderate height, have a significant impact on sediment movement and the evolution of the shoreline at both El Bajito and El Morro.

T_p shows considerable importance, as seen in Fig. 7b, where there is significant variability in wave periods. Although wave heights are not high, longer periods indicate greater wave energy, affecting the waves' ability to transport sediments and modify the shoreline. On the other hand, variables related to Stokes drift (SDX and SDY) show lower importance in the model, suggesting that at El Bajito and El Morro, the direct impact of these drifts on SLD is limited compared to the combined effect of waves and SL.

The order of importance of the variables is similar for both beaches, El Bajito and El Morro, although with greater magnitudes at El Morro. This may be due to the different geographical exposure of the two beaches. El Morro is more exposed to the open sea, which could amplify the effects of wave action and SL on SLD. In contrast, El Bajito, located on Tumaco Island, is protected by Bocagrande Island, which may moderate the impact of waves and tides in this area. This difference in exposure may explain why the same variables have a greater influence at El Morro, where hydrodynamic and wave conditions can act more intensely on the coastline.

The use of the RF model proved to be an ideal tool for understanding the processes and the most important variables influencing SLD on the beaches of El Morro and Bajito. This allowed for a more comprehensive understanding that not only considers ENSO climatic events but also coastal forcing as the main factor of SLD. The model not only helped measure the importance of these variables but also predicted SLD under mesotidal conditions and with H_s of up to 1.5 m, according to temporal evolution. The results showed a low error in the analysis of the average of the two beaches compared to the spatial resolution of the LANDSAT images used (30 m) This versatile and innovative method indicates that SL and Θm are the main factors representing greater variability in SLD.

Table 1
Random forest importance in ShoreLine Displacement (SLD).

Variable	El Bajito Beach		El morro Beach	
	Inc Node Purity	Relative Importance	Inc Node Purity	Relative Importance
Sea Level (SL)	1,241,083	9.21	879,294	10.58
Wave Direction (Θm)	1,231,286	9.14	797,590	9.6
Peak Wave Period (T_p)	1,098,880	8.15	792,510	9.54
Wind Wave Direction (WWD)	978,872	7.26	722,460	8.7
Significant Wave Height (H_s)	813,532	6.04	550,666	6.63
Mean Wave Period (MWP)	420,536	3.12	261,137	3.14
Wind Wave Significant Height ($H_{s\_}WW$)	313,914	2.33	191,114	2.3
Wave Direction at Variance Spectral Density Maximum (WVP)	244,342	1.81	173,715	2.1
Stokes Drift X Velocity (SDX)	179,408	1.33	118,693	1.43
Stokes Drift Y Velocity (SDY)	134,743	1	83,110	1

4. Conclusions

The calibration and validation process of the 2D FLOW & and result comparison of SWAN results in Delft3D using Waverys reanalysis data as an alternative to in-situ measurements demonstrated that, even with limited information, it is possible to successfully apply a coupled model to simulate hydrodynamic and wave conditions in the Tumaco region. The results showed a high correlation and low RMSE when comparing observed and simulated water levels.

The results obtained through CoastSat reveal a predominant trend towards accretion on the beaches of El Morro and El Bajito in Tumaco, which could initially be interpreted as a positive sign for the stability of these coasts. However, the presence of accretion should not lead to a false sense of security. For El Bajito beach, 64 % of the transects (1 to 7) show accretion, which might be temporarily compensating for erosion effects. This does not eliminate the need for long-term mitigation measures, especially since the remaining 36 % of transects (8 to 11) exhibit erosion. This area is also characterized by high poverty levels, making it particularly vulnerable to future coastal changes if not properly addressed. Similarly, on El Morro beach, 84 % of the transects (1 to 12, 16, 17, and 18) present accretion, while the remaining 16 % (transects 13 to 15) are experiencing erosion. The eroding section of El Morro includes the main tourist area, where hotels and restaurants are located, and erosion here could have significant socio-economic impacts. Therefore, while accretion may currently dominate in these beaches, both the vulnerable communities in El Bajito and the tourism infrastructure in El Morro require careful monitoring and proactive management to mitigate future risks.

Given the situation in El Bajito, where informal settlements, poverty, and poor land-use planning prevail, the implementation of traditional mitigation measures such as beach nourishment or nature-based solutions may not be feasible due to the lack of available space. Instead, medium- to long-term efforts should focus on adapting the built environment. This could involve improving housing conditions, reinforcing, and upgrading the stilt houses (palafitos) currently present in the area. Such adaptations would help to strengthen the resilience of the community against the ongoing threats of erosion and coastal flooding.

The results of the RF model indicate that SL and Θm are the most influential variables in SLD on the beaches of El Morro and El Bajito. This prominence over other variables, such as T_p and H_s, suggests that, in the context of Tumaco, fluctuations in SL and Θm play a more decisive role in coastal erosion and accretion. The relatively low observed wave heights, generally below 1.1 m, and wave periods that do not exceed 20 s imply that wave energy in this region is not sufficient to cause significant chronic erosion. The higher importance scores observed for El Morro compared to El Bajito may be attributed to its greater exposure to open sea conditions, whereas El Bajito benefits from natural protection by surrounding islands.

As a recommendation for future research, the predictive framework should be expanded to incorporate integrated process-based metrics, particularly the alongshore and cross-shore components of wave energy flux, which could synthesize the combined action of H_s, T_p, and θm in coasts with more pronounced energy gradients. Furthermore, the inclusion of anthropogenic variables (coastal land use, shoreline defenses, dredging, and alterations in sediment supply) and climate-forcing factors such as sea-level rise (SLR) would allow for a zone-specific assessment of the relative contributions of physical, human, and climatic drivers to coastal evolution and risk scenario.

CRediT authorship contribution statement

Andrés M. Enríquez-Hidalgo: Writing – original draft, Investigation, Formal analysis, Data curation. **Andrés Vargas-Luna:** Writing – review & editing, Supervision, Investigation, Conceptualization. **Marc Mestres:** Supervision. **Jorge Escobar-Vargas:** Supervision, Conceptualization. **Manuel Espino Infantes:** Supervision. **Andrés Torres:** Writing – review & editing, Validation, Supervision, Investigation, Formal analysis, Data curation, Conceptualization.

Declaration of competing interest

None.

Acknowledgements

The authors would like to express their gratitude to the Centro de Investigaciones Oceanográficas e Hidrográficas del Pacífico (CCCP) of the Dirección General Marítima (DIMAR) of Colombia for providing the data collected during their measurement campaigns, which were essential for configuring the model applied in this study.

They are also grateful to the Fondo Fundación WWB Colombia for their financial support for fieldwork activities in the development of the doctoral thesis "Decision Support System for Coastal Management in Response to Flooding and Coastal Erosion: A Case Study of Tumaco-Nariño," of which this article is a part.

The authors extend their sincere thanks to Minciencias | Ministerio de Ciencia, Tecnología e Innovación, for their support through the Fondo de Ciencia, Tecnología e Innovación del Sistema General de Regalías, which facilitated the selection of eligible projects to be approved by the OCAD. This work benefited from the Program of Doctoral Excellence Scholarships, aimed at training Colombian professionals at the doctoral level in Colombian higher education institutions, within the framework of the Bicentennial Doctoral Excellence Scholarship Program, as defined in Article 45 of Law 1942 of 2018.

Finally, they express their gratitude to the Instituto Javeriano del Agua, the Doctoral Program in Engineering, and the Master's Program in Hydrosystems of the Pontificia Universidad Javeriana for their valuable contributions in terms of material resources, including equipment, personnel, and financial support, which made the collection of primary data for this research possible.

Data availability

Data will be made available on request.

References

Alcaldía Municipal de Tumaco, 2008. Plan de Ordenamiento Territorial 2008–2019.

Alfaro-Chavarría, H., Zumbado-González, J., Mora-Escalante, R., Calleja-Apéstegui, F., Govaere-Vicarioli, G., 2023. Waves data in Costa Rica: validating the Waverys reanalysis using waves data. Ingeniería. Revista de la Universidad de Costa Rica 33 (2). https://www.redalyc.org/journal/441/44174486007/html/.

Arjasakusuma, S., Kusuma, S.S., Saringatin, S., Wicaksono, P., Mutaqin, B.W., Rafif, R., 2021. Shoreline dynamics in East Java Province, Indonesia, from 2000 to 2019 using multi-sensor remote sensing data. Land 10 (2). https://doi.org/10.3390/land10020100. Article 2.

Billet, C., Alonso, G., Danieli, G., Dragani, W., 2024. Evaluation of beach nourishment in Mar del Plata, Argentina: an application of the CoastSat toolkit. Coast. Eng. 193, 104593. https://doi.org/10.1016/j.coastaleng.2024.104593.

Bonaldo, D., Antonioli, F., Archetti, R., Bezzi, A., Correggiari, A., Davolio, S., De Falco, G., Fantini, M., Fontolan, G., Furlani, S., Gaeta, M.G., Leoni, G., Lo Presti, V., Mastronuzzi, G., Pillon, S., Ricchi, A., Stocchi, P., Samaras, A.G., Scicchitano, G., Carniel, S., 2019. Integrating multidisciplinary instruments for assessing coastal vulnerability to erosion and sea level rise: lessons and challenges from the Adriatic Sea, Italy. J. Coast. Conserv. 23 (1), 19–37. https://doi.org/10.1007/s11852-018-0633-x.

Bryant, M.A., Bryant, D., Provost, L., Hurst, N., McHugh, M., Wargula, A., Tomiczek, T., 2022. Wave Attenuation of Coastal Mangroves at a Near-Prototype Scale (ERDC TR-22-17). US Army Corps of Engineerss. https://apps.dtic.mil/sti/citations/AD1181016.

Cano, C., 2020. Gestión del Riesgo en Desastres en los Procesos de Planificación del Desarrollo Territorial en Comunidades del Pacifico Colombiano, Estudio de Caso Zona Urbana, Municipio de Tumaco. Departamento de Nariño. Universidad de Manizales.

Cano Calvo, C., 2021. Gestión del riesgo en desastres en los procesos de planificación del desarrollo territorial en comunidades del pacifico colombiano. Estudio de Caso Zona urbana, Municipio de Tumaco, Departamento de Nariño. https://ridum.umanizales.edu.co/handle/20.500.12746/4883.

Castelle, B., Scott, T., Brander, R.W., McCarroll, R.J., 2016. Rip current types, circulation and hazard. Earth Sci. Rev. 163, 1–21. https://doi.org/10.1016/j.earscirev.2016.09.008.

Choo, Y.M., Chun, K.H., Jeon, H.S., Sim, S.B., 2021. A predictive model for estimating damage from wind waves during coastal storms. Water 13 (9). https://doi.org/10.3390/w13091322. Article 9.

Chowdhury, R.R., Uchida, E., Chen, L., Osorio, V., Yoder, L., 2017. Anthropogenic drivers of mangrove loss: Geographic patterns and implications for livelihoods. In: Rivera-Monroy, V.H., Lee, S.Y., Kristensen, E., Twilley, R.R. (Eds.), Mangrove Ecosystems: A Global Biogeographic Perspective: Structure, Function, and Services. Springer International Publishing, pp. 275–300. https://doi.org/10.1007/978-3-319-62206-4_9.

Davenport, C., 2021. Effects of Bathymetry, Wave Environment and Sea Level on Rip Current Dynamics in a Wave-resolving Model [Thesis, University of Otago]. https://ourarchive.otago.ac.nz/handle/10523/11934.

de Andrade, T.S., de Sousa, P.H.G.O., Siegle, E., 2019. Vulnerability to beach erosion based on a coastal processes approach. Appl. Geogr. 102 (November 2018), 12–19. https://doi.org/10.1016/j.apgeog.2018.11.003.

De Goede, E.D., 2020. Historical overview of 2D and 3D hydrodynamic modelling of shallow water flows in the Netherlands. Ocean Dyn. 70 (4), 521–539. https://doi.org/10.1007/s10236-019-01336-5.

Delft University of Technology, 2006. SWAN Technical Documentation—Version 40.51. Delft University of Technology.

Deltares, 2022a. Delft3D-Hydro-Morphodynamics (Versión 4.05).

Deltares, 2022b. Delft3D-WAVE User Manual (Versión 4.05).

Djouder, F., Boutiba, M., 2017. Vulnerability assessment of coastal areas to sea level rise from the physical and socioeconomic parameters: case of the Gulf Coast of Bejaia, Algeria. Arab. J. Geosci. 10 (14), 299. https://doi.org/10.1007/s12517-017-3062-5.

Enríquez-Hidalgo, A.M., Lara-Borrero, J., Torres, A., 2022. Identification of explanatory factors of the presence and quantification of endocrine disruptors in commercially available bottled waters. Water Environ. J. 36 (1), 30–42. https://doi.org/10.1111/wej.12752.

Enríquez-Hidalgo, A.M., Vargas-Luna, A., Torres, A., 2025. Evaluation of decision-support tools for coastal flood and erosion control: a multicriteria perspective. J. Environ. Manag. 373, 123924. https://doi.org/10.1016/j.jenvman.2024.123924.

Espinoza Villacís, E., González Muñoz, R., Martillo Bustamante, C., Saltos Andrade, I., 2023. Modeling and analysis of wave transformation in the Bay of Santa Elena-

Ecuador in the period 2016-2020. Acta Oceanográfica del Pacífico 5 (1), 11–32. https://doi.org/10.54140/raop.v3i2.64.

Fogarin, S., Zanetti, M., Dal Barco, M.K., Zennaro, F., Furlan, E., Torresan, S., Pham, H. V., Critto, A., 2023. Combining remote sensing analysis with machine learning to evaluate short-term coastal evolution trend in the shoreline of Venice. Sci. Total Environ. 859, 160293. https://doi.org/10.1016/j.scitotenv.2022.160293.

Garge, N.R., Bobashev, G., Eggleston, B., 2013. Random forest methodology for model-based recursive partitioning: the mobForest package for R. BMC Bioinform. 14 (1), 125. https://doi.org/10.1186/1471-2105-14-125.

Genuer, R., Poggi, J.-M., Tuleau-Malot, C., 2015. VSURF: an R package for variable selection using random forests. R J. 7 (2), 19–33.

Gomez, M.L.A., Adelegan, O.J., Ntajal, J., Trawally, D., 2020. Vulnerability to coastal erosion in the Gambia: empirical experience from Gunjur. Intern. J. Disast. Risk Reduct. 45 (December 2019), 101439. https://doi.org/10.1016/j.ijdrr.2019.101439.

Houghton, T., Olmo, M.E., Mestres, M., Cos, P., Soret, A., Espino, M., 2025. Future wave climate in the NW Mediterranean from multi-model CMIP6 wind projections. In: Implications for the Ebro Delta (NE Spain). https://doi.org/10.22541/essoar.174690711.18439942?commit=9992f2a4a9b05dd70afc2e0e9d16b49e46c6873e.

IDEAM, 2020. Pronóstico de pleamares y bajamares en la costa pacífica colombiana (ISBN 958-95850-6-X). http://www.ideam.gov.co/documents/21021/137239/CARTILLA+PACIFICO+2020/882b155a-eafa-4380-8abe-33857240e8be?version=1.1.

Idier, D., Bertin, X., Thompson, P., Pickering, M.D., 2019. Interactions between mean sea level, tide, surge, waves and flooding: mechanisms and contributions to sea level variations at the coast. Surv. Geophys. 40 (6), 1603–1630. https://doi.org/10.1007/s10712-019-09549-5.

Juan, N.P., Rodríguez, J.O., Valdecantos, V.N., 2024. Comparison of the SIMAR-WANA, ERA-5, and Waverys databases for maritime climate estimations and the implications of coastal protection structures. J. Waterw. Port Coast. Ocean Eng. 150 (1), 04023021. https://doi.org/10.1061/JWPED5.WWENG-2017.

Kadigi, R.M.J., Robinson, E., Szabo, S., Kangile, J., Mgeni, C.P., De Maria, M., Tsusaka, T., Nhau, B., 2022. Revisiting the Solow-Swan model of income convergence in the context of coffee producing and re-exporting countries in the world. Sustain. Futur. 4. https://doi.org/10.1016/j.sftr.2022.100082.

Law, C., Aouf, L., Levier, A., Dalphinet, 2023. Quality Information Document Global High Resolution Production Centre GLOBAL_MULTIYEAR_WAV_001_032.

Li, J., Knapp, D.E., Lyons, M., Roelfsema, C., Phinn, S., Schill, S.R., Asner, G.P., 2021. Automated global shallow water bathymetry mapping using Google earth engine. Remote Sens 13 (8). https://doi.org/10.3390/rs13081469. Article 8.

Lin, L., Pussella, P., 2017. Assessment of vulnerability for coastal erosion with GIS and AHP techniques case study: southern coastline of Sri Lanka. Nat. Resour. Model. 30 (4), e12146. https://doi.org/10.1111/nrm.12146.

Marsooli, R., Orton, P.M., Mellor, G., Georgas, N., Blumberg, A.F., 2017. A coupled circulation-wave model for numerical simulation of storm tides and waves. J. Atmos. Ocean. Technol. 34 (7), 1449–1467. https://doi.org/10.1175/JTECH-D-17-0005.1.

Martins, K.A., de Souza Pereira, P., Silva-Casarín, R., Nogueira Neto, A.V., 2017. The influence of climate change on coastal Erosion vulnerability in Northeast Brazil. Coast. Eng. J. 59 (02), 1740007. https://doi.org/10.1142/S0578563417400071.

Martos, A., Isabel, A., 2022. The Gulf of Cadiz as a Natural Laboratory for the Validation and Exploitation of Coastal Altimetry and Model Data [Doctoral thesis]. https://rodin.uca.es/handle/10498/28930.

Morris, R.L., Boxshall, A., Swearer, S.E., 2020. Climate-resilient coasts require diverse defence solutions. Nat. Clim. Chang. 10 (6). https://doi.org/10.1038/s41558-020-0798-9. Article 6.

Mullick, Md.R.A., Tanim, A.H., Islam, S.M.S., 2019. Coastal vulnerability analysis of Bangladesh coast using fuzzy logic based geospatial techniques. Ocean Coast. Manag. 174, 154–169. https://doi.org/10.1016/j.ocecoaman.2019.03.010.

Mury, A., Collin, A., Houet, T., Alvarez-Vanhard, E., James, D., 2020. Using multispectral drone imagery for spatially explicit modeling of wave attenuation through a salt marsh meadow. Drones 4 (2). https://doi.org/10.3390/drones4020025. Article 2.

Niño, D., Oviedo, F., 2018. Determinación de la variación morfológica costera de la Bahía de Tumaco, a partir de análisis multitemporal con sensores remotos. Boletín Científico CIOH 36, 71–86. https://doi.org/10.26640/22159045.439.

Ortega, S., Osorio, A.F., Agudelo, P., 2013. Estimation of the wave power resource in the Caribbean Sea in areas with scarce instrumentation. Case study: Isla Fuerte, Colombia. Renew. Energy 57, 240–248. https://doi.org/10.1016/j.renene.2012.11.038.

Otero, L.J., Restrepo, J.C., Gonzalez, M., 2014. Tsunami hazard assessment in the southern Colombian Pacific basin and a proposal to regenerate a previous barrier island as protection. Nat. Hazards Earth Syst. Sci. 14 (5), 1155–1168. https://doi.org/10.5194/nhess-14-1155-2014.

Paulus, R., Dewals, B.J., Erpicum, S., Pirotton, M., Archambeau, P., 2013. Innovative modelling of 3D unsaturated flow in porous media by coupling independent models for vertical and lateral flows. J. Comput. Appl. Math. 246, 38–51. https://doi.org/10.1016/j.cam.2012.07.032.

Pollard, J., Spencer, T., Brooks, S., 2019. The interactive relationship between coastal erosion and flood risk. Progr. Phys. Geogr. Earth Environ. 43 (4), 574–585. https://doi.org/10.1177/0309133318794498.

Pramanik, S., Mandal, S., Shee, A., Halder, S., Sil, S., 2019. Tidal circulation studies using regional model in the Bay of Bengal. In: Murali, K., Sriram, V., Samad, A., Saha, N. (Eds.), Proceedings of the Fourth International Conference in Ocean Engineering (ICOE2018). Springer, pp. 829–836. https://doi.org/10.1007/978-981-13-3119-0_55.

Rivas, M., Luna, P., Lizarazo, J., 2019. Analytical fragility assessment of structures subjected to earthquake and tsunami loads: a case study on the colombian pacific coast. Tecnia 29 (2), 169–173. https://doi.org/10.21754/tecnia.v29i2.699.

Romero-Martín, R., Sanuy, M., Jiménez, J.A., 2025. Unveiling the role of storm surges as a driver of flooding on the western Mediterranean: a case study of the Ebro Delta. Nat. Hazards 121 (4), 4961–4984. https://doi.org/10.1007/s11069-024-06984-5.

Schipper, E.L.F., Revi, A., Preston, B.L., Carr, E.R., Eriksen, S.H., Fernández-Carril, L.R., Glavovic, B., Hilmi, N.J.M., Ley, D., Mukerji, R., de Araujo, M.S.M., Perez, R., Rose, S.K., Singh, P.K., 2022. Climate resilient development pathways. In: Pörtner, H.-O., Roberts, D.C., Tignor, M.M.B., Poloczanska, E.S., Mintenbeck, K., Alegría, A., Craig, M., Langsdorf, S., Löschke, S., Möller, V., Okem, A., Rama, B. (Eds.), Climate Change 2022: Impacts, Adaptation and Vulnerability. Contribution of Working Group II to the Sixth Assessment Report of the Intergovernmental Panel on Climate Change. Cambridge University Press.

Siders, A.R., Keenan, J.M., 2020. Variables shaping coastal adaptation decisions to armor, nourish, and retreat in North Carolina. Ocean Coast. Manag. 183, 105023. https://doi.org/10.1016/j.ocecoaman.2019.105023.

Son, S., Lynett, P., Ayca, A., 2020. Modelling scour and deposition in harbours due to complex tsunami-induced currents. Earth Surf. Process. Landf. 45 (4), 978–998. https://doi.org/10.1002/esp.4791.

Stronkhorst, J., Levering, A., Hendriksen, G., Rangel-Buitrago, N., Appelquist, L.R., 2018. Regional coastal erosion assessment based on global open access data: a case study for Colombia. J. Coast. Conserv. 22 (4), 787–798. https://doi.org/10.1007/s11852-018-0609-x.

Sun, W., Liang, B., Shao, Z., Wang, Z., 2022. Analysis of Komen scheme in the SWAN model for the whitecapping dissipation during the tropical cyclone. Ocean Eng. 266, 113060. https://doi.org/10.1016/j.oceaneng.2022.113060.

Tamiminia, H., Salehi, B., Mahdianpari, M., Quackenbush, L., Adeli, S., Brisco, B., 2020. Google Earth engine for geo-big data applications: a meta-analysis and systematic review. ISPRS J. Photogramm. Remote Sens. 164, 152–170. https://doi.org/10.1016/j.isprsjprs.2020.04.001.

Tejada, C., 2003. Clima marítimo y dinámica litoral de la bahía de Tumaco, datos básicos para la evaluación de riesgos ambientales marinos. 10 (Boletín Científico CCCP), pp. 83–96.

Tejada, C., Otero, L., Castro, L.Á., Afanador, F., Solano, J., Morales, A., Fonseca, A., 2003. Aportes al Entendimiento de la Bahía de Tumaco: Entorno Oceanográfico, Costero y de Riesgos (Diseño y producción: Editorial Sepia Ltda). www.editorialsepia.cominfo@editorialsepia.com.

Valderrama-Landeros, L., Flores-Verdugo, F., Flores-de-Santiago, F., 2022. Assessing the coastal vulnerability by combining field surveys and the analytical potential of CoastSat in a highly impacted tourist destination. Geographies 2 (4), 642–656. https://doi.org/10.3390/geographies2040039.

van Dongeren, A., Ciavola, P., Martinez, G., Viavattene, C., Bogaard, T., Ferreira, O., Higgins, R., McCall, R., 2018. Introduction to RISC-KIT: resilience-increasing strategies for coasts. Coast. Eng. 134, 2–9. https://doi.org/10.1016/j.coastaleng.2017.10.007.

Viñes, M., Sánchez-Arcilla, A., Epelde, I., Mösso, C., Franco, J., Sospedra, J., Abalia, A., Líria, P., Grifoll, M., Ojanguren, A., Hernáez, M., González, M., Sánchez-Arcilla, A., 2025. Morphodynamic predictions based on machine learning. Performance and limits for pocket beaches near the Bilbao port. Front. Environ. Sci. 13. https://doi.org/10.3389/fenvs.2025.1600473.

Vledder, G., Zijlema, M., Holthuijsen, L., 2011. Revisiting the JONSWAP bottom friction formulation. In: Proceedings of the International Conference on Coastal Engineering; No 32 (2010): Proceedings of 32nd Conference on Coastal Engineering, Shanghai, China, 2010.; waves.41, Vol. 1. https://doi.org/10.9753/icce.v32.waves.41.

Vos, K., Harley, M.D., Turner, I.L., Splinter, K.D., 2023. Pacific shoreline erosion and accretion patterns controlled by El Niño/southern oscillation. Nat. Geosci. 16 (2), 140–146. https://doi.org/10.1038/s41561-022-01117-8.

Wang, J., Wang, Y., 2022. Evaluation of the ERA5 significant wave height against NDBC buoy data from 1979 to 2019. Mar. Geod. 45 (2), 151–165. https://doi.org/10.1080/01490419.2021.2011502.

Wen, S., Zhang, F., Wang, Z., Li, F., Jing, X., Zhao, J., 2019. Coastal Erosion monitoring and Hazard degree assessment at Penglai Sandy coast based on remote sensing. IOP Conf. Ser. Earth Environ. Sci. 234 (1), 012014. https://doi.org/10.1088/1755-1315/234/1/012014.